HHS Public Access

Author manuscript

J Comp Neurol. Author manuscript; available in PMC 2017 June 16.

Published in final edited form as:

J Comp Neurol. 2017 June 15; 525(9): 2050–2074. doi:10.1002/cne.24155.

The organization of frequency and binaural cues in the gerbil inferior colliculus

Gilberto David Graña[1], **Kendall A. Hutson**[1], **Alexandra Badea**[2], **Andrew Pappa**[1], **William Scott**[1], and **Douglas C. Fitzpatrick**[1]

[1]Department of Otolaryngology-Head and Neck Surgery, University of North Carolina at Chapel Hill, Chapel Hill, North Carolina

[2]Center for In Vivo Microscopy, Duke University Medical Center, Durham, North Carolina

Abstract

The inferior colliculus (IC) is the common target of separate pathways that transmit different types of auditory information. Beyond tonotopy, little is known about the organization of response properties within the 3-dimensional layout of the auditory midbrain in most species. Through study of interaural time difference (ITD) processing, the functional properties of neurons can be readily characterized and related to specific pathways. To characterize the representation of ITDs relative to the frequency and hodological organization of the IC, the properties of neurons were recorded and the sites recovered histologically. Subdivisions of the IC were identified based on cytochrome oxidase (CO) histochemistry. The results were plotted within a framework formed by an MRI atlas of the gerbil brain. The central nucleus was composed of two parts, and lateral and dorsal cortical areas were identified. The lateral part of the central nucleus had the highest CO activity in the IC and a high proportion of neurons sensitive to ITDs. The medial portion had lower CO activity and fewer ITD-sensitive neurons. A common tonotopy with a dorsolateral to ventromedial gradient of low to high frequencies spanned the two regions. The distribution of physiological responses was in close agreement with known patterns of ascending inputs. An understanding of the 3-dimensional organization of the IC is needed to specify how the single tonotopic representation in the IC central nucleus leads to the multiple tonotopic representations in core areas of the auditory cortex.

Graphical Abstract

Correspondence: Gilberto David Graña, Department of Otolaryngology/Head and Neck Surgery, The University of North Carolina at Chapel Hill, 101 Mason Farm Road, Campus Box #7546, Chapel Hill, NC 27599. gdgrana@unc.edu.

CONFLICT OF INTEREST

The authors declare no conflicts of interest from any sources with regard to the subject and conduct of this study.

AUTHOR CONTRIBUTIONS

All authors had full access to all the data in the study and take responsibility for the integrity of the data and the accuracy of the data analysis. Study concept and design: DCF. Acquisition of data: GDG, KAH, AB, DCF. Analysis and interpretation of data: GDG, KAH, DCF. Drafting of the manuscript: GDG, KAH, DCF. Critical revision of the manuscript for important intellectual content: GDG, KAH, DCF. Statistical analysis: GDG, KAH, DCF. Obtained funding: DCF.

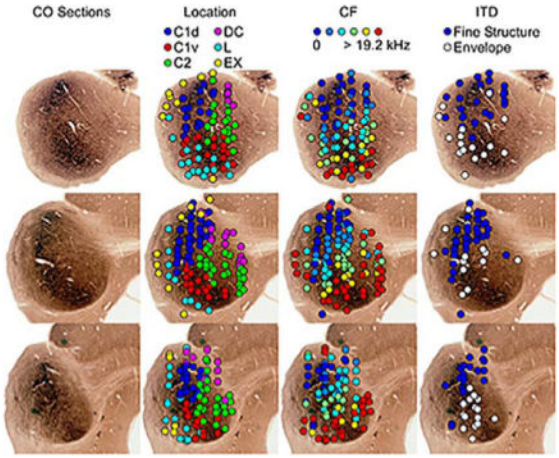

The MRI of a gerbil brain was used to align physiological data from the inferior colliculus on a tissue atlas, graphically illustrating the original locations of recording sites and the organization of characteristic frequencies and interaural time di3erences.

Keywords

interaural time differences; binaural processing; frequency map; latency; RRID: SCR_001622; RRID: SCR_014199; RRID: SCR_003070

1 INTRODUCTION

The central nucleus of the inferior colliculus (IC) is the common target of separate ascending pathways that convey discrete types of auditory information (for reviews, see Hutson, 1997; Winer & Schreiner, 2005; for more recent studies, see Malmierca, Saint Marie, Merchan, & Oliver, 2005; Cant & Benson, 2006, 2008; Loftus, Bishop, & Oliver, 2010; Cant, 2013; Felix, Magnusson, & Berrebi, 2015). From there, the information is relayed to the ventral division of the medial geniculate body (MGv) of the thalamus, which in turn projects to multiple core regions of the auditory cortex, including the primary auditory cortex (AI). A transformation from an organization based on frequency to one according to function occurs between the level of the IC and the auditory cortex. This transformation is best shown in the mustached bat, where neurons with different physiological properties and functional roles, such as sensitivity to target range or relative velocity, are arrayed according to their position in the tonotopic map of the IC central nucleus (Wenstrup, Mittmann, & Grose, 1999; Portfors & Wenstrup, 2001). However, at the level of the cortex, neurons are clustered into functional areas characterized by a common response type (O'Neill & Suga, 1979; Suga, O'Neill, Kujirai, & Manabe, 1983; Fitzpatrick, Suga, & Olsen, 1998). In other mammals, the isofrequency laminae in the IC become multiple tonotopic regions in the cortex. Functional parcellation of the cortical areas is likely, such as into "place" and "pattern" pathways (Malhotra, Hall, & Lomber, 2004; Lomber & Malhotra, 2008; Recanzone & Cohen, 2010; Rauschecker, 2015), but the details of these functional areas are less clear than in the mustached bat. In addition, in the mustached bat the change from an organization according

to frequency to one according to function occurs in the output pathways of the IC, so that the thalamic organization resembles that seen in the cortex (Olsen & Suga, 1991a, 1991b; Wenstrup, Larue, & Winer, 1994; Wenstrup & Grose, 1995; Wenstrup, 1999; Pearson, Crocker, & Fitzpatrick, 2007). In other species, the connection from the IC to the thalamus is typically presented as a single pathway, and the output from the thalamus as branching to innervate separate cortical areas (Kaas & Hackett, 2000; Winer & Schreiner, 2005). These relationships are schematized in Figure 1. Other than in the mustached bat, path-ways from the IC to the thalamus are not typically described in terms of both physiological and functional roles—in part due to the lack of identified "information-bearing parameters" that relate specific responses and neuronal location to a functional role. An exception is sensitivity to interaural time difference (ITD), which is an information-bearing parameter for sound location as well as for improving signal detection in noise.

Processing of ITDs in terms of neurophysiology and behavior is among the most studied properties of the auditory system (Bernstein, 2001; Konishi, 2003; Palmer & Kuwada, 2005; Vonderschen & Wagner, 2014). Most of the physiological focus has been on identifying the specializations used in pathways from the auditory nerve to the superior olivary complex (SOC) to encode and extract the ITD information with microsecond resolution. Less attention has been paid to localization of ITD-sensitive neurons within the pathways from the IC to the cortex than to the physiological properties of the neurons. Here, we used gerbils to study the localization of ITD sensitivity within the IC. Previous studies on gerbil ITD sensitivity have described the pathways to the IC from the main nuclei of the SOC that convey ITD information (Cant & Benson, 2006; Cant, 2013). In the present study, localization was achieved through the use of an MRI atlas whereby physiological information across cases could be plotted within a common framework. This framework will then form the basis for further physiological and connectional studies of the thalamus and cortex, to help distinguish whether the patterns of connections observed in the mustached bat are a specialized adaptation to their particular lifestyle, or are representative of a common mammalian plan.

2 MATERIALS AND METHODS

2.1 Experimental procedures

Thirty-five female gerbils, weighing between 50 and 70 g, were used for this study. The animals were handled and housed according to the standards described by the National Institutes of Health Committee on Care and Use of Laboratory Animals. The experimental protocols were approved by the Institutional Animal Care and Use Committee at the University of North Carolina at Chapel Hill.

2.1.1 Surgery and animal handling—Animals were anesthetized with an intramuscular injection of ketamine/xylazine (100 mg ketamine and 4 mg xylazine per kg body weight), supplemented with one-third the original dose every 60 min. Animals were transferred to a double-walled, sound-attenuated booth, where each recording experiment lasted 6 to 8 hr. The head was shaved and secured to a stereotactic platform with a bite-bar of dental cement molded to the teeth of a gerbil's skull. In this configuration, the orientation of the gerbil's

brain resembles that shown in Figure 2a. To avoid puncture of the transverse sinus (ts), the head holder was inclined 15° (nose up), resulting in the orientation in Figure 2b. Corneas were protected with sterile lubricating eye ointment (Refresh P.M.), and temperature was maintained at approximately 37°C with a heating blanket and rectal probe. A subcutaneous injection of xylocaine was administered under the scalp and regions adjacent to the external auditory meatus. The scalp was incised and retracted, and blunt dissection was continued laterally to expose the junction of the internal and external acoustic meatus on both sides of the head. The external meatus was opened to allow insertion of a small plastic tube for stimulus delivery. The stimulus tubes were sealed in place with connective tissue. The plastic tubes were attached to individual (left and right) speakers to complete a sealed stimulus delivery system.

A small hole was drilled in the skull to access the IC. For each penetration, a parylene-coated tungsten microelectrode (5 or 12 MΩ; A-M Systems, Sequim, WA) was positioned at predetermined coordinates relative to lambda and advanced into the brain until robust multiunit responses to a 70- to 80-dB SPL frequency sweep were observed. The electrode was advanced through the IC and responses recorded until no auditory activity could be demonstrated, at which point a lesion was created in the tissue by applying a +5-μA current for 2 to 5 s to mark its location and assist in reconstructing the penetration trajectory. The electrode was then withdrawn and repositioned at a different set of coordinates, and the procedure for locating recording sites was repeated. All recordings were obtained from the left IC. Stimulus presentation and neural spike-time recording procedures are detailed below.

2.1.2 Recording procedures and acoustic stimulation—The electrode was advanced by a Burleigh Inchworm micro-drive (6000ULN, Burleigh Instruments, Victor, NY) capable of moving in sub-micron increments. A Grass P15 AC preamplifier was used for recording, with filters set between 300 and 3000 Hz and a gain of 1,000; additional gain was provided by an amplifier external to the booth (Signal Recovery model 5113, AMETEK, Burwyn, PA). Spike times from a window discriminator (Frederick Haer, Bowdoinham, ME) were stored digitally (Tucker Davis RZ6, Alachua, FL).

Stimulus waveforms were generated in a custom MATLAB (http://www.mathworks.com/; RRID: SCR_001622) program running on a Windows 7 PC platform. The stimuli were sent to a TDT (Alachua, FL) multi I/O processor (RZ6), where outputs for left and right channels went to programmable attenuators (TDT PA5), then to a headphone driver (TDT HB7), and finally to Beyerdynamics (Heilbronn, Germany) speakers (DT48, 8 Ω) attached to the plastic tubes in each ear. Stimuli were calibrated using a Bruel & Kjaer (Naerum, Denmark) ¼-in. microphone with a short probe tube attachment, and corrections for levels at different frequencies were made online. Stimulus levels are expressed in dB sound pressure level (SPL).

Stimuli consisted of tone bursts to measure frequency tuning, threshold, and binaural responses. Responses to ITDs were probed first with binaural beats to low-frequency tones or to sine amplitude modulated (SAM) tones at 100% modulation depth, to test for ITD sensitivity to the ITD_{FS} or ITD_{ENV}, respectively. The test for ITD_{FS} was most commonly used for neurons with low characteristic frequencies (CFs) while the test for ITD_{ENV} was

most often used for neurons with high CFs. Fine-structure stimuli used low frequencies from 200 to 1,700 Hz, with a 1- or 3-Hz binaural beat frequency, with equal levels of 50 or 70 dB SPL at each ear. Modulation frequencies were tested with SAM tones at CF, and often with a level difference of 10 to 40 dB between the ears, with the ipsilateral ear typically having the higher intensity. Additional tests of ITD sensitivity included static ITDs with low frequency tones or noise. The noise could be presented as correlated or anticorrelated at each ear.

During the experiment, the full set of analyses was available online from the MATLAB routines for display, enabling stimuli to be chosen with knowledge of a unit's ongoing response characteristics. This approach helped to reduce the parameters of a large potential stimulus space.

2.1.3 Tissue processing—At the conclusion of each recording session, animals were euthanized with an overdose of Nembutal (100 mg/kg), and perfused through the heart with 0.1 M phosphate buffer rinse (pH 7.4) followed by 4% para-formaldehyde in the same buffer. The head was removed and placed overnight in fixative at 4°C. The following day the head was repositioned in the head holder, and the brain was blocked in the same plane as the electrode penetration. The brain was then dissected from the skull and placed in 30% sucrose phosphate buffer until it sank. Brains were then frozen-sectioned at 40 μm and reacted for levels of mitochondrial activity using histochemistry for CO activity (Wong-Riley, 1976). After the reaction was terminated, sections were rinsed, mounted on glass slides, cleared, and coverslipped for microscopic reconstruction of the penetration and to plot the location of unit recording sites relative to the location of the lesion. Photographs of the sections were obtained using a Zeiss Axioskop microscope with a Canon Rebel TI1 camera and software (Melville, NY), and combined using Photoshop (http://www.adobe.com/photoshop/; RRID: SCR_014199) to produce full-section images.

2.2 Physiological data analysis

Responses were displayed online on an oscilloscope, and single units, when present, were identified and studied in detail. Units that met a criterion of having spike intervals <0.7 ms occurring in <1% of all intervals were verified to be single units. Although single unit recordings were taken as they were encountered during each penetration, for purposes of mapping the IC, a recording was always made—regardless of whether it was single or multiunit—at approximately 200-μm intervals beginning from the first recorded response. In the event of multiunits, the discriminator level was lowered until multiunit activity was recorded.

2.2.1 Frequency tuning, threshold, and latency—The CF was determined from responses to tone bursts varying in frequency and intensity, typically starting at 70 dB SPL, decreasing in 20-dB steps until there was no response, and then increasing in 5- or 10-dB steps until the response just returned. The CF of a unit was the frequency that produced a response at the lowest stimulus intensity. The threshold value was determined from a "neurometric function" (Kiang & Moxon, 1974; Day, Koka, & Delgutte, 2012), where the responses in stimulus intervals exceeded those in nonstimulus intervals by $d' = 1$. Because most binaural stimuli were presented at suprathreshold levels, we also determined the best

frequency at 70 dB SPL (BF70), i.e., the frequency that produced the maximal response at 70 dB SPL. Latency was taken as the median time from the stimulus onset to the first spike in the response at BF70 and 70 dB SPL.

2.2.2 Binaural response type—The basic scheme of Irvine (1992) was used to define binaural response types. Units were defined by their response to stimuli presented to each ear alone as excitatory (E), inhibitory (I), or no response (O). The binaural response (BR) type was defined based on the relationship to the monaural responses as either facilitation (F, 20% greater than the sum of responses to each ear) or I (20% less than the response to either ear). Otherwise, if the binaural response fell between these two extremes, the relationship was labeled as occlusion (O). To classify a unit, the designations were written as [contralateral][ipsilateral]/[binaural]; thus, for example, a unit that had an excitatory response at both ears and a facilitative binaural response would be classified as EE/F. We categorized a neuron as monaural if we ran the following three binaural tests with no effect on response: 1) responses at CF and/or BF70 tested separately and together across a series of common stimulus levels, 2) responses to the responding ear held at CF and 10 to 20 dB above threshold while levels to the opposite ear were varied, and 3) at least one test of ITD sensitivity (see below), typically a binaural beat to a tone or modulation frequency.

2.2.3 ITD sensitivity—The most common test of ITD sensitivity used a binaural beat stimulus, which consists of tones presented to each ear that differ in frequency (Kuwada, Yin, & Wickesberg, 1979). The frequency difference produces a continuous change in interaural phase. If the frequency difference is small (usually 1 to a few Hz, but in some cases up to ~100 Hz), neurons in the IC can follow this changing phase, because of the specialized circuits that collect and enhance the phase-locking produced by hair cells and the auditory nerve. Sensitivity to the binaural beat can occur to the fine structure of low-frequency sounds or to the envelopes of sounds including high-frequency carriers, as has been shown in many species (Kuwada, Stanford, & Batra, 1987; Batra, Kuwada, & Stanford, 1989, 1993; Yin & Chan, 1990; McAlpine, Jiang, & Palmer, 1996; Marshall et al., 2008), including gerbils (Spitzer and Semple, 1993, 1995). We used the analytic procedures described by Yin & Kuwada (1983a) to quantify the responses of ITD-sensitive neurons. The responses to binaural beat fine structure (ITD_{FS}) or envelope (ITD_{ENV}) were used to generate delay curves, or rate changes as a function of ITD to different stimulus or modulation frequencies. The average of all the delay curves is called a composite curve, which was used to determine the neuron's best ITD (Bitd) as the peak of the composite curve. The average interaural phase of response to each frequency was calculated from cycle histograms binned on the beat frequency (typically 1 or 3 Hz), and the slope of the plot of interaural phase versus frequency was the neuron's characteristic delay (CD) and the intercept was the neuron's characteristic phase (CP).

While interaural phase is a measure of the timing differences in phase-locking between the two ears, vector strength (VS) is a measure of the strength of phase-locking. The VS equals 1 when all spikes occur at a particular phase and 0 when the spikes are distributed evenly across all phases (Goldberg & Brown, 1969). From the binaural beat stimuli, it is possible to extract the VS to the beat frequency, as well as to the stimuli presented to each ear (e.g.,

1,000 Hz in one ear and 1001 in the other, or SAM tones that differ by 1 Hz in modulation frequency), by binning the cycle histograms at each frequency in turn. Then, the VS from the frequency at each ear can be used to predict the VS obtained to the beat frequency, as a test of whether the recorded neuron could be a site or primary binaural interaction or has inherited the ITD sensitivity from a previous stage of extraction of the phase-locked timing information (Yin & Kuwada, 1983b; Kuwada et al., 1987; Batra, Kuwada, & Fitzpatrick, 1997). The significance of the VS and interaural phase was determined from the Rayleigh test of uniformity (Mardia & Jupp, 2000, criterion $P<0.001$). Finally, the best frequency for ITD sensitivity (BFitd) was determined as the weighted average of a plot of synchronized rate (product of VS and spike rate) for each frequency or modulation frequency where the VS was significant (Fitzpatrick, Kuwada, & Batra, 2000; Fitzpatrick, Roberts, Kuwada, Kim, & Filipovic, 2009).

Sensitivity to ITDs could also be tested with other stimuli. Neurons that did not respond to binaural beats could be tested with static ITDs, where the ITD at a single frequency (or noise) was varied in steps (50–100 μs for ITD_{FS}, up to 1 ms for ITD_{ENV}). It was not possible to sample all possible frequencies, ITDs, and levels, so values were chosen that were most likely to identify ITD sensitivity, if it existed, based on other responses that were collected. A positive result was therefore a clear indication of ITD sensitivity, but a negative result cannot be an absolute indication of lack of ITD sensitivity.

2.3 MRI-based reconstructions

The MRI of a gerbil brain served as a framework for aggregating physiological data obtained from different animals. MR images of the head of a 13-week-old, 65-g female Mongolian gerbil was obtained from the Center for In Vivo Microscopy (CIVM) at Duke University (http://www.civm.duhs.duke.edu/). The techniques were similar to those used to produce a mouse brain atlas suitable for use in histological and genotyping experiments (Johnson et al., 2002a; Johnson, Cofer, Gewalt, & Hedlund, 2002b; Badea, Johnson, & Williams, 2009). Briefly, enhanced MR images were obtained through the use of ProHance (Bracco Diagnostic, Princeton, NJ), a gadoteridol-based contrast agent, mixed with a 10% buffered formalin fixative. The fixed brain was then imaged using a 9.4-T magnet with a GE Excite console (Epic 11.0, GE Healthcare, Milwaukee, WI), using a 3D spin echo sequence with a repetition time (TR) of 50 ms and an effective echo time (TE) of 6.2 ms. The resulting image array was 1,024 × 2,048 × 1,024 pixels over a field of view of 22 × 44 × 22 mm, and data were reconstructed at an isotropic resolution of 21.5 μm.

Using this MRI brain to catalogue experimental observations involves basic steps that are general to any similar study, and then specific implementations of each step for the material specific to this study. The basic steps are 1) rotating the stack of MRI images so that the orientation of the region of interest matches that seen in the histological images, so that MRI images corresponding to each histological section can be identified; 2) morphing the matching MRI images to the region of interest in each histological section; 3) plotting or digitizing points to be localized from the histology onto the morphed MRI images; and 4) reversing the morphing of the MRI image so that the plotted locations are within the

framework of the atlas brain. In the following paragraphs, we discuss each step in more detail for our particular experiment.

2.3.1 Standardized orientations of the MRI images—The stack of images in the MRI brain were viewed in ImageJ (Rasband, 1997–2014, RRID: SCR_003070), where the set could be manipulated as a volume with a variety of tools to zoom, rotate, or orient in different planes. A plugin, TransformJ (Meijering, 2000–2002), allowed free rotation of the stack about the three Cartesian axes, using the centroid of the image stack as the origin of rotation. The orientation of the imaged brain was first adjusted to have the midline be vertical in any horizontal or coronal section when displayed on the computer screen; this corrected for errors in the "yaw" and "roll" of the brain in the stack, respectively. The "pitch"—the angle of the head when looking up and down—was chosen to be 0° when the pons and ventral surfaces of the temporal lobes were coplanar, similar to how the brain is positioned when removed from the head for horizontal sectioning. All angles of rotation reported subsequently are in relation to this *standard orientation*. The stack was then cropped one last time to produce a volume with pixel dimensions 1,024 (mediolateral) × 1,024 (dorsoventral) × 1,650 (anteroposterior), leaving enough room in front of and behind the gerbil's head so that rotation of the stack would not crop pixels pertaining to the gerbil's skull or brain.

The procedures necessitated the identification of a coordinate system with a zero that is visible as a discrete point in the MRI. We chose the location of lambda—the intersection of the lambdoidal and sagittal fissures—as the nominal zero of our coordinate system; a point visible on the skull is useful both during physiological experiments and when displaying coordinates in anatomical sections. A photograph of a gerbil skull is shown in Figure 3a, illustrating the locations of lambda and bregma, another common landmark. In Figure 3b and c, the close correspondence between the landmarks on the skull and in the MR images is apparent after the pitch of the MR brain is adjusted to bring lambda and bregma into the same horizontal and sagittal planes. For rotation procedures, the nominal zero was the geometric center of the image stack. The final coordinates are all stored and referenced relative to the location of lambda as it appears in the standard orientation, however. Examples of sections taken in the coronal, sagittal, and horizontal planes from the standard orientation are shown in Figure 3d, e, and f, respectively.

2.3.2 Mapping electrode penetrations in MRI space—To align information from the physiological experiments into the MR framework, the MR-imaged brain was oriented to match the plane of the histological sections for each case. To achieve this, the MR stack was rotated iteratively to visually match features in the histological material. It proved to be important that the angles be determined from parts of sections local to the IC, because once the brain was removed it could sag and distort differentially, such that a single plane of section would not apply to the entire brain. In adjusting the pitch of the MRI, the most useful features identified were the relative positions of the caudal end of the commissure of the IC and the caudal junction where the IC joins the brainstem (both left and right; see Figure 3d and e, the latter of which is in the sagittal plane); when adjusting yaw, the procedures primarily relied on the relative sizes of the IC, especially the caudal sections not attached to

the brainstem. The final angles were recorded and stored into a database file created for each experiment.

For the fitting procedure, the pitch of the MR stack was altered in 5° steps until a rough approximation of the histological sections was achieved; changes were then made in 1° steps until a best match was found. A nominal 1° level of precision corresponds to an error of approximately 34 μm over the depth of the IC (~2 mm). Corrections in yaw were performed similarly, but started with 1° changes since deviations in coronal symmetry were intentionally made small during the physical blocking of the brain. As a control for observer bias and to estimate the reproducibility of this method, the angle of section was determined in four brains independently by two observers. One of the rotation angles was identical between observers, one differed by 1°, and two differed by 2°.

Once the plane of section was known, each histological section of interest—those that contained the electrode penetrations—were mapped to individual MR sections. The photograph of a histological section was opened in Photoshop along with the corresponding MR image, which was added as a separate image layer. The MR section was then scaled independently in the X (width) and Y (height) dimensions until the edges of the IC in the MRI matched those of the histological section; as with determining the angle of section for the MRI, the alignment works best by focusing only on the region of interest (here the IC) instead of the tissue section as a whole. The fitting was performed on a section-by-section basis; the scaling factors required for each section were typically similar for any given case. If there were large nonlinear distortions between a histological section and its corresponding MR image, the alignment was further refined using a piece- wise linear geometric transformation in MATLAB.

The locations of the recording sites along each electrode penetration were plotted relative to the lesion(s) made and the track of the penetration through the sections. The course of a penetration could typically be seen as a light or dark streak through the brain, depending on whether there was blood present. The distance from the lesion was determined from the micrometer reading of recording sites obtained during the experiment, and corrected for shrinkage based on a scaling factor from the morphed brain.

The recording locations were converted to corresponding coordinates in the MR framework space by applying the inverses of the morphing transformations described above. The resulting coordinates represent the locations of the recorded units relative to the nominal zero point of the MRI brain described earlier. The coordinates of the recording sites in MRI space and their respective data analyses were stored in an Excel database file in combination with the anatomical location of each unit in the IC and its physiological response properties. In this manner, all the data sets became coregistered within a single MR framework.

2.3.4 Test for localization error—To estimate the expected range of location errors in the procedures, a test case was prepared where two penetrations were made through a brain at different angles, leaving behind a small cylindrical hole on each side. To do this, an anesthetized animal was placed in the head holder, and a 29-gauge, thin-walled tube was lowered into the left tectum; the angle of the head holder was then changed by 10° and a

second tube was lowered on the right side. The animal was then perfused with both tubes in situ. We chose to penetrate the superior colliculus (SC) rather than the IC to ensure that the fiduciary marks coursed through the entire depth of the midbrain and to avoid the possibility of the tubes exiting the IC prior to completing the penetration (note the curvature of the caudal margin of the IC in Figure 2). After perfusion the tubes were removed, and the brain was sectioned in the horizontal plane and prepared with cytochrome oxidase (CO) histochemistry. Section alignment proceeded as above, but the person performing the stretching procedures and reconstruction in MRI space was blind to the penetration angles involved. After alignment, the coordinates of the centers of each of the holes, for each section, were determined using imaging software in MATLAB and converted to MRI space coordinates. Once the coordinates were obtained, a best-fit line (using orthogonal regression) was used to estimate both the dispersion of the centers around the line and the angles of penetration, all in the sagittal plane (Figure 4; standard error of the estimate: 2.25 for the left hole and 2.43 pixels for the right). The scatter around the best-fit line had a range of 5 pixels (corresponding to 105 μm in the MRI brain) and a standard deviation of 1.91 pixels (~40 μm in MRI space). The estimated angles relative to a sagittal orientation were 16.4° for the left penetration and 5.64° for the penetration on the right. The reconstructed angle difference was 10.76°, compared with the nominal 10° change in the stereotaxic frame.

2.3.5 Additional orientations of the MRI used in this study—We designated two histological preparations to act as “reference atlases” to help visualize the pooled locations of our recording sites and their physiological properties against the patterns of CO activity found in the different parts of the IC. One series was cut in the plane of the electrode penetrations and will thus be referred to as the “physiological” orientation. The other was cut in the near-horizontal plane relative to the standard. The two atlas series were aligned to the MRI, and their angles of section were stored as in the other cases. A GUI was developed in MATLAB to visualize the locations of our recording sites onto these sections; once a series of images was loaded, the coordinates of our recordings were transformed from the MRI space into the “space” of a given reference atlas. Additional elements of the GUI allowed individual recording sites to be selected, their physiological properties examined in detail, and the reconstructed positions within their own histological section viewed. The orientations of these two atlases, combined with views derived from the standard orientation of our MRI framework, served as the basis for visualizing recording site locations and physiological properties in this paper.

3 RESULTS

A total of 386 single and multiunit recordings were obtained from the IC of 35 gerbils. Single units were recorded at 47% of locations. The inclusion of multiunits did not distort the overall patterns or affect the significance of the statistics compared with when single units were tested separately, so the results were pooled. Except where noted, the illustrated examples are from single units.

3.1 Examples of physiological results

The major categorizations of neurons in the gerbil's IC were based on frequency tuning and binaural response, particularly ITD sensitivity. Figure 5 shows two examples of ITD-sensitive neurons. The neuron in Figure 5a–e was tuned to low frequencies with a CF of 841 Hz (a), thus falling within the range of strong phase-locking found at the periphery. It was strongly facilitated by binaural stimulation, with only a small response to each ear alone (b). Consequently, the binaural classification for this neuron was EE/F. Delay curves generated by a 1-Hz binaural beat show sensitivity to ITD_{FS} that aligned near the peaks across frequency (c). When the delay curves were averaged, the Bitd from the composite curve was −190 μs (d). When phase was plotted as a function of frequency (e), the CD (−240 μs) was close to the Bitd, and alignment near the peaks resulted in a CP near zero (0.03) cycles. The BFitd was 734 Hz, i.e., similar to the CF.

Figure 5f–j shows a neuron with a CF higher than the phase-locking range (4,000 Hz). This neuron was strongly driven by contralateral tones at CF (g). There was no response to the ipsilateral stimulus, but the response to the contralateral ear was nearly completely inhibited by binaural stimulation, indicating an inhibitory ipsilateral input. Thus, this neuron was classed as EO/I. The delay curves generated from a 1-Hz binaural beat of the envelopes of SAM tones showed strong sensitivity to ITD_{ENV} that aligned at the troughs across modulation frequency (h). The composite curve had a minimum near zero ITD (i) and a Bitd of −2,600 μs. The plot of interaural phase versus modulation frequency (j) yielded a CD of 77 μs and a CP of nearly $^1/_2$ (−0.47) cycles. The BFitd was to a modulation frequency of 144 Hz (not shown, see Materials and Methods).

The two examples in Figure 5 demonstrate responses that can only have originated through the circuitry of the SOC that extracts the ITD information. The responses of the two neurons to stimuli at each ear and the alignment of ITD curves across frequencies further separate them as receiving inputs primarily from the medial superior olive (MSO; Figure 5a) or lateral superior olive (LSO; Figure 5b).

Figure 6 shows two neurons that were not ITD sensitive. The neuron in Figure 6a–c had a CF of 8,000 Hz (a). This neuron had an excitatory response to the contralateral ear, no response to the ipsilateral ear, and was slightly inhibited by stimulation of both ears, compared with contralateral alone (b). The inhibition from the ipsilateral side was confirmed when the contralateral response was held at a constant level and the ipsilateral level was varied (c). Consequently, this neuron was classed as EO/I. This neuron showed no ITD sensitivity to the binaural beat with SAM tones at CF (tested with two intensity combinations), or to noise. The neuron in Figure 6d–f had a CF of 5,700 Hz. Like the previous neuron, it was strongly excited by contralateral stimulation, but in this case there was no response or change in the response to ipsilateral stimulation (E and F). It was therefore classified as EO/O. This neuron also showed no ITD sensitivity to several tests, so by these criteria it was considered a "monaural" rather than "binaural" neuron.

3.2 Parcellation of the gerbil's IC

Based on CO histochemistry (Figure 7), the gerbil IC is easily divisible into two basic regions: a central or "core" nucleus encapsulated by a cortical or "belt" region. The central nucleus was divided into a lateral crescent-shaped region showing the highest CO activity (C1) and a medial region with lighter CO activity (C2). Furthermore, C1 has the appearance of dorsal and ventral subdivisions, which we refer to as C1d and C1v, respectively. Surrounding the central nucleus were cortical regions, including (at the level shown in Figure 7) the dorsal cortex (DC) and lateral cortex, which included the external and lateral nucleus (EX and L, respectively). Of the surrounding regions, the DC had the lightest CO reaction in the IC, while the L had a density similar to that of C2 in the central nucleus. The EX was distinctive, being composed of islands of high CO reactivity embedded within fiber tracts, indicated by arrows in Figure 7b (see Chernock, Larue, & Winer, 2004), forming the most dorsal and lateral margin of the IC.

3.3 Recovery of recording sites

Figure 8 shows penetrations through the middle third of the IC in three different animals at different mediolateral locations. Each penetration and recording site was recovered in a section treated for CO histochemistry (a–c) and plotted relative to a lesion or pair of lesions made during the penetration (arrows). All three penetrations started with low CF neurons and progressed systematically to neurons with high CFs (see corresponding plots, c–f). The same graphs illustrate ITD sensitivity for each unit. The presence of ITD sensitivity is indicated by a filled rather than open circle, and sensitivity to ITD_{FS} is shown in blue and ITD_{ENV} in cyan. The most lateral penetration (Figure 8a) was mainly through C1, except for the last unit, which was in the L. All the units in the dense CO of C1 were ITD-sensitive, either to the ITD_{FS} or ITD_{ENV}. The middle penetration (Figure 8b) started in the C1d, traversed C2, entered C1v, and ended in L. The units in C1d and C1v were ITD-sensitive, while the units in C2 and L were not. The most medial penetration (Figure 8c) started in the DC, then entered C2, and then entered the dense zone of C1v. Only the first unit in this penetration was ITD-sensitive.

3.4 Physiology in different parts of the IC

The basic physiology in each part of the IC is shown in Table 1. Listed for each region are the numbers of units sampled and the percentage of units that were identified as monaural, binaural, and ITD-sensitive, with ITD sensitivity further divided into those responding to ITD_{FS} or ITD_{ENV}. The denominator for each category is the number in the *n* column. All regions of the IC had a preponderance of binaural neurons. Of the monaural neurons, the largest percentages were found in C1v and C2. Some ITD-sensitive neurons were found in each subdivision, but the proportions varied considerably. The overwhelming majority in C1 were ITD_{FS} neurons. Area C1v also had a high percentage of ITD-sensitive units, with most being ITD_{ENV} neurons. In contrast, relatively few units in C2 were sensitive to ITDs. In the cortical areas, a fairly large proportion of neurons was sensitive to ITDs, with ITD_{FS} sensitivity predominating in the DC and EX, and ITD_{ENV} in the L.

3.5 Distribution of response types across the IC

The locations of neurons are shown across the extent of the IC in Figures 9 and 10. In Figure 9, the CO labeling in five different anterior–posterior sections from our physiological atlas is shown in the first column, with A being the most caudal, and E the most rostral. This set of tissue acts as a 320-μm-spaced atlas on which physiological data can be compared, bearing in mind that each photomicrograph is a "snapshot" that represents the center of a 320-μm slab of tissue on which all physiological data within that slab are summarized. A small dot in the top left of each histological section is labeled with its corresponding coordinate in the standard MRI framework, representing mediolateral, dorsoventral, and caudorostral distance from the origin, respectively. The small inset image above Figure 9a shows a sagittal view of the gerbil brain from the standard MRI orientation, with the IC indicated near the center. The solid line through the IC indicates the estimated angle of section. In Figure 9f–j, the location of each recording site is shown reconstructed in the atlas brain with a color code depicting the location of each site as recovered from histological sections (Figure 8). There is good correspondence between location in the individual histological sections and in the pooled MRI atlas despite natural variations across subjects. There is also clear clustering by identified area. These properties indicate that the summed physiological data, mapped onto the MRI atlas brain, can be correlated with the histological observations across individual cases. A region where identification of location is difficult is in the rostral central nucleus. The regions of dense and light CO are compact, and distinctions between C1d and C1v in particular are difficult to assess.

In Figure 10, the distributions of CF, ITD sensitivity, and binaural type are shown. Within the central nucleus, the CF (f–j) progressed in an orderly fashion from dorsal to ventral, consistent with the individual penetrations shown in Figure 8. The tonotopy extended across both C1 and C2 in the central nucleus. Caudally the region was almost exclusively low frequency, while the rostral IC contained the full range of frequencies despite its compact architecture. Outside of the central nucleus the tonotopy was less distinct.

ITD sensitivity (Figure 10k–o) was separated into whether the sensitivity was to the ITD_{FS} or ITD_{ENV}. The majority of ITD_{FS} units were in C1d while ITD_{ENV} units were found primarily in C1v, but there were also ITD-sensitive neurons of both types in C2, as well as in each of the nuclei outside of the central nucleus. The separation of the two ITD types was in large part governed by the time constraints of the experiments, so that low CF neurons were usually tested and characterized in terms of ITD_{FS} and high CF neurons for $ITD_{ENV.}$ This frequency selectivity is a major reason for the dichotomy between ITD_{FS} neurons in C1d and ITD_{ENV} neurons in C1v, and tests for both types were not performed. Overall, C1v was more complex than C1d because a greater proportion of non-ITD–sensitive neurons was seen.

The regional distribution of binaural sensitivity (EE, EI or monaural; Figure 10p–t) suggests at least a partial segregation based on these binaural classes. The categories are broad, with, for example, the EE designation corresponding to EE/O, EE/F, EO/F, OO/F, OE/F, and EE/occlusion. However, they do capture the general effect of whether the *ipsilateral* input was excitatory, inhibitory, or absent. In the central nucleus, the EE neurons were generally dorsal to EI neurons, and the monaural neurons tended to be located more ventrally as well.

Despite these trends, there was considerable intermingling of binaural types. In particular, there were EI neurons in the C1d that were ITD-sensitive (e. g., Figure 10s), where most neurons had low CFs and were preferential to ITD_{FS} (Figure 10n).

To compare the clustering of frequency and ITD, the Classifier Learner App in MATLAB (r2015b) was used. The CFs of neurons were separated into three groups, low (<2,000 Hz), medium (≥2,000 to <16,000), and high (≥16,000), and the ITD sensitivity into two groups (yes or no). The "response" data was the group (either frequency or ITD) while the "predictors" were the X, Y, and Z coordinates of the neurons in the MRI brain coordinates. The classifier used was the linear support vector machine. In some cases a nonlinear fit (e.g., weighted k-nearest neighbor) was superior, but more often such fits were worse, so to avoid cherry-picking among models the single model was applied. The main focus was on neurons in the central nucleus, so the sample was 261 neurons. In the frequency comparison, the clustering according to location based on frequency had an accuracy of 89% and the average d' was 1.94, with a d' of 1 typically used as a threshold for discriminability. For ITD, the accuracy of the classifier was 74% and the d' was 1.3. Thus, both frequency and ITD representations were separable within the central nucleus.

3.6 Representation of parameters of ITD sensitivity

Using the binaural beat, the alignment of delay curves occurs across frequency provides a separation that, to a first approximation, equates to the inputs as being from the MSO or LSO (Figure 5). However, in addition to peak-type neurons with a CP near zero and trough-type neurons with a CP near 0.5 (Figure 5), there were also intermediate-type neurons with a CP near 0.25. Thus, the distribution of CP is a continuum rather than pure categories. Furthermore, in some neurons the phase-frequency plot was nonlinear, and the bestfit line did not adequately portray the combination of delay curves that produced the composite curve. In these cases, the CP was computed from the slope of the frequencies that dominated the composite curve. For the ITD_{FS}, peak-type neurons were the most numerous, with intermediate-type less abundant and trough-type the least (Table 2). The relationships between the parameters are incorporated in the formula: Predicted Best ITD =CD +(CP/BFitd) (Fitzpatrick et al., 2000; Shackleton, McAl-pine, & Palmer, 2000; Hancock & Delgutte, 2004; Grothe, Pecka, & McAlpine, 2010). Using this formula, the correlation between the predicted and actual best ITDs was 0.91. As expected from the formula, the best ITD therefore increased in the three groups along with the CP. The CD, in contrast, varied relatively little. The change in Bitds was significant (F, df, and *P* values in Table 2, using two-way ANOVAs where the effect of group was tested against the value in question), as was, by definition, the change in CPs. In contrast, the change in the CDs was not significant. These relationships indicate that the delays, or CDs, of the different types of neurons are comparable, but the alignment across frequency and the frequency content itself varies. The BFitds were similar across types and the standard deviations were large. Consequently, the differences in frequency tuning that led to ITD sensitivity in the three classes of CP were not significant.

Another feature of interest is the sharpness of tuning to ITDs. The VS is a measure of sharpness that is not affected by the manner in which the responses vary across frequencies,

as is the case with composite curves or noise-delay curves. Many of the maximum VS values recorded across neurons were very high, above 0.9 in 15/52 neurons, and even above 0.95 in 9 neurons. On average, both the maximum and mean VS values were higher in intermediate-type neurons, compared with either peak- or trough-type. This effect of ITD type was significant in the ANOVA.

For the ITD_{ENV} the trends were quite different (Table 3). As with the ITD_{FS}, all three types were represented. However, instead of peak-type neurons being the most common, trough-type neurons prevailed. Because the ITD sensitivity was to low-frequency envelopes (10–800 Hz was typically tested), the range of ITDs covered was extremely wide (Bitds in Table 3), and the width of tuning in individual neurons was broad (Figure 4b). As with the ITD_{FS}, the range of CDs was smaller than the range of Bitds, and did not differ between the groups. However, the mean values of CP for the intermediate-type neurons were near the edge of the trough-type, rather than the edge of the peak-type. The VS values were lower, and there was no trend for the intermediate-type neurons to have sharper tuning to ITDs.

Additional comparisons between ITD_{FS} and ITD_{ENV} sensitivity are made in Figure 11. The difference in the range of frequency tuning available to extract the ITD is shown in Figure 11a. There is overlap between the two ranges such that the total range for ITD sensitivity extends from the lowest envelope frequency (10 Hz and presumably lower), to >1,000 Hz for ITD_{FS}. Figure 11b shows the ability of IC neurons to phase-lock to the input frequencies at each ear compared with phase-locking to the binaural beat frequency. For neurons that extract the ITD directly from the phase-locked inputs, the VS to the binaural beat frequency (VSitd) is expected to be related to the VS of inputs from both the contralateral (right) and ipsilateral (left) ear, expressed as VSr × VSl. All VS values can be obtained from the responses to the binaural beat stimulus (see Materials and Methods). We considered a monaural-to-binaural ratio (i.e., (VSr × VSl)/VSitd) or (contralateral × ipsilateral)/binaural that was greater than 0.8 as evidence of a unit's potential as a primary site of binaural interaction (Kuwada, Fitzpatrick, Batra, & Ostapoff, 2006); the number of neurons that meet this criterion are plotted against their ITD frequency (fine structure) or modulation frequency (envelope) in Figure 11b. Virtually no IC neurons met this criterion for ITD_{FS}, but the criterion was often met for the lowest ITD_{ENV} frequencies. Sensitivity to these low frequencies is thus potentially available as a primary binaural interaction site at the level of the IC (but see Discussion).

We found ITD-sensitive neurons in all regions of the IC. However, most of them were from the central nucleus, and specifically C1, or the regions of densest CO reaction product that we separated as C1d and C1v (Table 1). To test for spatial organization of the ITD-sensitive parameters within C1, we again used the Classifier Learner App in MATLAB (r2015b). The classifier showed spatial clustering of ITD_{FS} and ITD_{ENV} neurons (83% accuracy, d' =1.8, n =108). This result largely reflects the fact that ITD_{FS} stimuli were used with low CF neurons and ITD_{ENV} stimuli with high CF neurons. When separated into three groups of CP corresponding to the peak, trough, and intermediate types of Tables 2 and 3, the classifier failed to discriminate any location for intermediate-type neurons, classifying all as either peak- or trough-type neurons (n =69, reduced from 108 cases where ITD_{FS} or ITD_{ENV} could be determined, but in some cases data for the binaural beat were insufficient for analysis).

This pattern makes sense if intermediate-type neurons are equally likely to be found near either peak- or trough-type neurons. Consequently, we did further analysis excluding the intermediate-type neurons. In this case, a spatial organization for the peak and trough response types was indicated, as well as for Bitd and BFitd (all >80% accuracy, d's >1.8). In contrast, the CDs could not be distinguished between the peak and trough type groups (65% accuracy, $d' = 0.68$).

Finally, since the above contrasts are at least in part a reflection of the initial ITD_{FS} and ITD_{ENV} distinction, the next model tested was to compare the parameters just for ITD_{FS} neurons. There were too few trough-type neurons in this group for the CP analysis, but the CD, Bitd, and BFitd analyses all failed to show a spatial organization of these parameters (<70% accuracy, $d' < 0.7$, $n = 40$).

3.7 Other response features

Other responses recorded for most neurons included BF70 and Q70, latency, threshold at CF, and peristimulus time histogram (PSTH) type. Some of these, such as PSTH, are too varied to describe here. For all areas, the range of latencies was wide, extending from about 5 to 50 ms. In a one-way ANOVA there was a significant effect of area. The main effect was due in part to the presence of particularly long average latencies in EX, but was also present when EX was removed. When considered separately, the latencies among core areas were not significantly different, nor were the latencies among belt areas. However, on average, latencies were on the order of 4 ms longer in belt areas than core areas (14.4 vs. 10.7 ms), and we deemed six regional comparisons as significant (using an adjusted alpha level of $P < 0.005$ for significance in multiple *t*-test comparisons): EX versus the three core areas, L versus C1v and C2 (but not C1d), and DC versus C1v only. Other features that varied according to core versus belt were BF70 (higher in some belt areas, such as L), and Q70 (wider in the belt areas). The BF70s were generally lower than the CFs, as expected from the half-octave shift in the region of the basilar membrane, excited by high rather than low intensities.

3.8 Further use of the MRI atlas

A useful feature of the pooled data in the MRI atlas is that it can be sectioned to fit other planes, and used to visualize data in different orientations. In Figure 12, cell locations (f–j), characteristic frequency (k–o), and ITD sensitivity (p–t) are plotted against five different dorsoventral sections from the horizontally cut reference image atlas (see Material and Methods; 12a is the most dorsal section, while 12e is the most ventral) and using the same color coding as the previous histological atlas (Figures 9 and 10). The MRI-derived image above the first column again illustrates the angle of section determined for this case. As in the physiological orientation, the location data show good clustering, especially in the central nucleus, in accordance with the histological atlas.

Viewing the characteristic frequency in the horizontal plane illustrates the dorsolateral-to-ventromedial gradient of the tonotopy of the central nucleus. The ITD sensitivity panels show the expected preference for dorsal and lateral portions of the central nucleus to be sensitive to ITD_{FS} while ITD_{ENV} sensitivity is preferred in the ventral and medial locations.

In Figure 13, the physiological data are represented as surface plots in all three dimensions. Recording sites were grouped and color-coded based either on their locations in the IC (a–d), on their CF (e–h), or on the degree of ITD sensitivity (i–l) within the central nucleus. The coordinates were plotted in MATLAB in the MRI standard orientation; subsequently, each group of data was subject to a Delaunay triangulation, producing surfaces that were then exported to MIMICs for rendering. The composite triangulations are shown in a coronal view (Figure 13a,e,i; dorsal at the top, medial to the right, and rostral going into the page), a sagittal orientation viewing the lateral surface (Fig. 13b,f,j; caudal is to the right, dorsal is at the top, and medial going into the page), a sagittal view of the medial surface (Fig. 13c,g,k; rostral is to the right, and lateral is into the page), and a horizontal view (Fig. 13d,h, l; medial is to the right, rostral is at the top, and ventral is going into the page). The segregation of location data illustrated in Figures 9 and 12 can be seen here as integrated surfaces to better appreciate how the different regions fit together. Similarly, the three-dimensional gradient of the tonotopic axis of the central nucleus is apparent when visualized in these different orientations. The bottom panels organize the ICC by the percentage of cells that were ITD-sensitive in cubes with 320-μm sides. The region with the highest proportion of ITD-sensitive cells was coextensive with, but somewhat larger than, C1d. The region of medium numbers of ITD-sensitive neurons overlapped with C1v, and the region of few ITD-sensitive neurons overlapped with C2. In C1v and C2, the organization was largely orthogonal to the isofrequency laminae (Figure 13e–h).

4 DISCUSSION

This study described the representations of frequency and of ITDs, an information-bearing parameter for sound location and hearing signals in noise, at the level of the IC and in particular the central nucleus of the IC. Neural recordings in the gerbil's IC were combined with recovery of recording sites from CO-stained material, and the data were pooled, with computer assistance, into an atlas based on a high-resolution MRI scan of a normal gerbil brain; similar attempts to reference physiological data points to established atlases have been made by others (e.g., Semple & Aitkin, 1979). The results of our study indicate that the central nucleus has a single tonotopic organization that includes subregions that differ in their responses to ITDs. Surrounding the central nucleus are belt regions that are distinct from the central nucleus in terms of tonotopy, binaural response properties, latency, and/or CO activity. In general, the response distributions reflected the patterns of inputs as described in previous tract-tracing studies in the gerbil (Cant & Benson, 2003, 2006, 2008; Cant, 2013).

We describe the major features of the gerbil IC in terms of a central or core region surrounded by a cortical or belt region, and each can be subdivided based on CO activity levels (Figure 7). While further subdivision of the cortical region is possible in some preparations (e.g., Golgi stains; see Oliver & Morest, 1984 and Faye-Lund & Osen, 1985), such distinctions are, at best, tenuous based solely on CO-stained material. Furthermore, a common organizational plan at the level of the auditory cortex (and the MG) is a core region defined by a strict tono-topic organization surrounded by associated belt regions (Kaas & Hackett, 2000). In conforming to this anatomical arrangement, we consider the cortical

structures of the IC to be, at least to a first approximation, equivalent to the belt regions described at higher order locations.

4.2 Benefits of the MRI-based framework

A persistent problem in neuroanatomical and neurophysiological studies is that commonly used methods for plotting results are difficult to correlate across cases, histological procedures (e.g., different stains, section angles, or reactions), and laboratories. The main use of a standard frame of reference such as an MR-imaged brain is to facilitate comparisons in all of these situations. The subjective and objective tests suggest that the procedures introduce errors that on average are about 50 μm or less and not likely to exceed 100 μm. While Cant & Benson (2005) had previously published an extensive atlas of the gerbil IC using histological sections from all three dimensions, the use of an MRI-based atlas permits a less labor-intensive and more flexible means of comparison between cases, as the frame of the MRI reference can be freely rotated. In addition, since MRIs are obtained with the brain in situ, distortions inherent in histological procedures are normalized to an intact brain. Additional datasets, such as from connectional or immunocytochemical experiments, can be readily incorporated. Such examples have been presented in the literature for the mouse, perhaps the most comprehensive of which is the Allen Reference Atlas (Dong, 2008), which integrates multiple modalities including atlases and techniques produced at the Duke CIVM (Badea, Ali-Sharief, & Johnson, 2007; Johnson et al., 2010). The gerbil, because of its sensitivity to low frequencies, is a more suitable model than the mouse for many studies that are important for human hearing.

4.3 Organization of the gerbil's IC and relationship to input pathways

4.3.1 The core region: the central nucleus—The divisions of the IC were identified based on CO histochemistry and response properties of single and multiunit recordings. The main finding was the identification of a relatively separate domain of ITD sensitivity within the lateral region of the frequency laminae that corresponds to the regions of densest CO activity in the gerbil's IC. This work extends previous studies of CO histochemistry and input connections in the gerbil (Cant & Benson, 2006, 2008; Cant, 2013). Following injections into the IC, three types of input patterns based on retrograde labeling were found. Two of these were seen primarily following injections into the central nucleus: group 1 inputs included labeled cells in the cochlear nucleus (CN), the nuclei of the lateral lemniscus (nLL), and the MSO and LSO, while group 2 inputs included labeled cells in the CN and the nLL, but few if any from the SOC (Cant & Benson, 2006). The injection sites that showed SOC inputs (group 1) tended to be located in or near the lateral region of intense CO activity in the central nucleus. Within this region, a dorsal *pars lateralis* has been associated with strong inputs from the SOC (Cant, 2013). The injections with minimal SOC inputs (group 2) were typically located in the medial regions of the central nucleus. However, some injections into ventral regions of the dense CO activity, particularly the more ventral regions, were also group 2. Thus, there was an association, but not a strict correlation, between regions of dense CO and inputs from the MSO and LSO that should convey ITD information.

The physiological results corresponded closely to this pattern of ascending inputs. Most neurons sensitive to ITDs were in the region of dense CO activity, what we call C1. Cluster

analyses further showed ITD- and non–ITD-sensitive neurons to be separable. The pars lateralis, which receives dominant inputs from the MSO and the lateral (low-frequency) limb of the LSO (Cant, 2013), is essentially equivalent to our C1d, and, as would be expected, was strongly associated with low CFs, ITD_{FS} sensitivity, and excitation or facilitation from each ear. This class of responses is characteristic of that seen primarily in the MSO (Yin & Chan, 1990; Spitzer & Semple, 1995; van der Heijden et al., 2013; Plauska, Borst, & van der Heijden, 2016). In our results C1d extended nearly to the dorsal pole of the IC in caudal sections (Figure 9a,f), but its extent was less clear in the most rostral sections.

Neurons in C1v, or the ventral part of the high CO region, were distinguished from those in C1d because they had predominantly high CFs and the ipsilateral input was typically inhibitory. These are expected characteristics of responses from the medial, high-frequency limb of the LSO, which is also consistent with the connectional data (Cant & Benson, 2006, 2008; Cant, 2013). Many C1v neurons were sensitive to ITD_{ENV}, but whether these neurons also showed sensitivity to ITD_{FS} in the tails of their tuning curves was not tested. There was a proportion of neurons (10.6%) in C1v that were not binaural, and thus were unlikely to be driven by inputs from the LSO. This pattern of results also closely parallels that of the previous anatomical experiments, where most injections in the ventral region of dense CO had a group 1 pattern of inputs, but some had a group 2 pattern.

The medial part of the central nucleus, or C2, had less dense CO activity than C1, and was previously shown to have group 2 patterns of retrograde labeling (Cant & Benson, 2008). This area had a mixture of response types. Many C2 neurons either were not driven binaurally or were EI with ITD sensitivity not readily demonstrated. These responses are consistent with input pathways other than the MSO and LSO that can include the CN on both sides and monaural and/or binaural inputs from the nuclei of the lateral lemniscus. However, ITD sensitivity was not strictly confined to regions of highest CO activity, in that some neurons with low CFs but medial to the heaviest CO active regions were sensitive to the ITD_{FS} (e.g., compare G and H with L and M in Figure 10). Neurons sensitive to ITD_{ENV} were also observed out-side the boundaries of the highest CO activity.

4.3.2 The belt region: dorsal and lateral cortices—Injections of retrograde tracers in previous studies identified a third, or group 3, type of input to the cortical, or belt areas of the IC. Cases in this group showed a few labeled cells in the ascending pathway while inputs from the auditory cortex were more prevalent than for the central nucleus (Cant & Benson, 2006). Neurons in the cortical regions of the IC as a whole had a less distinct tonotopy and possessed, on average, longer latencies than were observed in the central nucleus. These and similar features characterize belt regions of the IC, and this structural organization can be traced back to its early origins in the opossum, a primitive mammal from which the basic “plan” for the mammalian auditory system is derived. In this species, the belt areas are also distinguished by their abundant descending inputs from cerebral cortex, whereas the core areas are primary targets of ascending projections from the CN and SOC (Willard & Martin, 1983).

In the gerbil, the borders of the L can be readily appreciated in all material prepared for CO histochemistry, where its lower activity level stands in contrast to the high levels of activity

characteristic of the central nucleus, especially C1. On its lateral side area L has a distinct border where it abuts the fibrous part of the EX. In rats and cats, injection of anterograde tracers into the dorsal cochlear nucleus (DCN) or anterior ventral cochlear nucleus (AVCN) shows a “winged” projection pattern in the IC, with one of the wings forming an extensive lamina in the central nucleus (and extending marginally into the DC), and the other being shorter and just lateral to the core area (Loftus, Malmierca, Bishop, & Oliver, 2008; Malmierca et al., 2008). Similar projections beyond the central nucleus have been reported in the gerbil (Moore & Kitzes, 1985; Cant & Benson, 2008). Thus, in some respects the L appears to have dual features—descending inputs from the cerebral cortex and ascending inputs from lower order auditory structures—that suggest it possesses both belt and core characteristics. Its outputs could help resolve the question. Most belt areas have stronger connections with the dorsal division of the MG than with the ventral division, in contrast to the central nucleus. The outputs of area L to the MG are not yet known. Physiologically, area L differed from the central nucleus by its average latency, although both had neurons with long latencies, up to about 45 ms. The tonotopy in the L had the same general pattern of low to high frequencies as did the central nucleus, but in general over-represented high frequencies. Overall, area L had the highest mean and median CFs of any area, and few units were sensitive to ITD_{FS}. These characteristics suggest that the L may have a greater affinity with either C1v or C2, rather than C1d.

Along the most lateral margin of the IC is the EX, consisting of islands of cells embedded within the fibrous capsule overlaying the IC, which eventually merges with the brachium of the IC. These cellular islands stain intensely for CO and positively for γ-aminobutyric acid (GABA) in rat (Chernock et al., 2004) and gerbil (personal observations). Thus, anatomical and physiological distinctions make the EX cells likely to be distinct from those of the L, rather than an extension of it. Response properties of neurons in the EX were varied; many were low frequency and ITD-sensitive, yet high-frequency and monaural neurons were also found. Because the cells were embedded in fiber tracts, the possibility of recording from fibers must be considered. However, many of the recordings in our sample of EX neurons were of single units held for a considerable period and were thus presumably cells; reconstructions were typically consistent with recordings from within the cellular islands.

The other part of the belt we identified was the DC, which together with the EX forms a shell covering the central nucleus along its dorsomedial and lateral margins, with the rostral and caudal cortex, completing the encirclement of the outer margin of the central nucleus except at its most ventromedial part where the central nucleus itself appears to form the border with the fibrous mantle beneath the IC. Most medially in the IC there was a region of nearly absent CO activity, where identification of DC was unambiguous. However, the transition from the DC to C2 was sometimes difficult to identify in the CO material, in contrast to each of the other regions, where the histological distinctions were relatively clear; indeed, we found this border to be the most difficult to resolve across all of our cases.

Finally, it should be noted that throughout the IC, there was a general trend of low frequencies being represented dorsally and high frequencies ventrally. In the dorsal parts of each area, whether EX, L, C1d, C2, or DC, neurons with low CFs, including some sensitive to ITD_{FS}, were found. These parallel representations are likely to form functional processing

units that loop between the IC and the auditory cortex. In particular, the ITD sensitivity in belt areas, particularly the EX and DC, could be derived from the cortex or from local loops within the IC, since they receive little input from the ascending pathways (Cant & Benson, 2006). That they are grouped together in broad outline suggests functional relationships between them.

4.4 Monaural and binaural neurons

In addition to the MSO and LSO, information from both sides comes from the superior paraolivary nucleus and dorsal nucleus of the lateral lemniscus (DNLL), and both CNs project directly to each IC. Axons arising from neurons within the central nucleus arborize locally not only in the core, but throughout the ipsilateral IC (Oliver, Kuwada, Yin, Haberly, & Henkel, 1991; Saldaña & Merchán, 1992; Malmierca, Hernandez, Antunes, & Rees, 2009; Wallace, Shackleton, & Palmer, 2012). Thus, there are abundant sources of binaural interactions possible in the IC, and it is not surprising that we, and others, have identified a large preponderance of binaural responses in all subdivisions of the IC (Aitkin, Webster, Veale, & Crosby, 1975; Popelar & Syka, 1982; Kelly, Glenn, & Beaver, 1991). Because of the complexity of such interactions and the varied response patterns they can create, we chose to focus our more detailed characterizations on the ITD-sensitive neurons.

In a sample of IC neurons, up to about 24% were likely to be monaural units, although 11.6% were “unconfirmed” in that the full battery of tests (both ears individually followed by tests of interaural level difference and ITD) was not completed. This proportion is in general agreement with the literature on gerbil (Semple & Kitzes, 1985; Bruckner & Rubsamen, 1995) and other species (Aitkin et al., 1975; Popelar & Syka, 1982; Kelly et al., 1991), although higher proportions of monaural units have also been reported (Wenstrup, Ross, & Pollak, 1986; Schreiner & Langner, 1988; McAlpine et al., 1996). One feature found in virtually all studies is an orderly increase in the proportion of monaural units as frequency increases (Schreiner & Langner, 1988; Kelly et al., 1991; Bruckner & Rubsamen, 1995; McAlpine et al., 1996), and this was true in our material as well. The fewest monaural units were found in the low-frequency–dominated C1d (median frequency 1.0 kHz), while the most were found in C1v (median 8.0 kHz) and C2 (median 7.4 kHz). Monaural neurons may receive their primary inputs directly from the contralateral CN, including stellate cells of the AVCN and fusiform and giant cells of the DCN. That neurons in the IC retain purely monaural properties suggests that processing of some spectral cues, to a degree, remains independent of binaural influences at the level of the IC.

4.5 Representation of ITDs in the central nucleus of the IC

The question of whether frequency tuning and distribution of ITD sensitivity and its parameters were spatially separable in the central nucleus was investigated using classifier training. The predictors were the X, Y, and Z coordinates, and the response was the frequency or ITD property for each recording site. This analysis indicated a spatial organization of CF (low, middle, or high) consistent with the tonotopy seen in the plots of the recording sites (Figure 10f–j). The property of ITD sensitivity was also significantly (d’ >1) affected by spatial location within the central nucleus. However, the overall organization of frequency versus tonotopy was not strictly orthogonal, as most low-CF neurons were

ITD-sensitive while fewer high-CF neurons were, so that the gradients of ITD sensitivity differed across frequency contours (Figure 13i–l). The gradients further indicated that C2 contains fewer ITD sensitive neurons than C1, and that C1v contained fewer than C1d, as expected from Table 2.

The finding of relatively separate functional domains in the central nucleus along an isofrequency lamina is consistent with previous anatomical, physiological, and immunohistochemical studies in many species. In cat, Roth, Aitkin, Andersen, & Merzenich (1978) used retrograde labeling techniques and hypothesized that the ICC is composed of anatomically, physiologically, and functionally distinct regions. This observation was confirmed and extended by Loftus, Bishop, Saint Marie, & Oliver (2004) and Loftus et al. (2010), who showed that the ascending projections from the CN, LSO, and MSO form multiple functional regions within the frequency lamina of the ICC and each lamina —a projection pattern not unlike those reported by Cant & Benson (2006) in the gerbil. This grouping of specific projection patterns to different groups of cells—the synaptic domain hypothesis (Oliver & Huerta, 1992)—was also demonstrated in rat and mouse using immunohistochemical studies to investigate GABA and glycine distribution in the ICC (Choy Buentello, Bishop, & Oliver, 2015). Our current results add to this growing body of evidence in support of the central nucleus as a composite structure of functional regions organized along a tonotopic axis.

Parameters of ITD sensitivity were obtained using tones of different frequencies presented as binaural beats, followed by an analysis for CP, CD, Bitd, and BFitd as developed by Yin and Kuwada (Kuwada et al., 1979; Yin, Chan, & Kuwada, 1983; Yin & Kuwada, 1983a, 1983b) and used in many later studies (McAlpine et al., 1996; Spitzer & Semple, 1998; Blanks, Roberts, Buss, Hall, & Fitzpatrick, 2007; Fitzpatrick, Roberts, Kuwada, Kim, & Filipovic, 2009). The classifier training was applied to the parameters of ITD sensitivity to investigate their spatial organization within C1 of the central nucleus, as determined by the density of CO reaction product. Within C1, the distribution of ITD_{FS} and ITD_{ENV} properties was spatially segregated, but, as we have mentioned, this was largely a property of frequency organization and experimental design, because low-CF neurons were generally tested with stimuli to probe ITD_{FS} and high-CF neurons with ITD_{ENV}. However, the fact that CP was spatially separable indicates that the designation of C1d and C1v is not purely nominal, but represents regions that receive ITD-sensitive inputs primarily from the MSO or LSO, respectively. Similar conclusions regarding clustering of CF and CP were derived from tetrode studies where neighboring single neurons were shown to have similar properties of CF and CP (Seshagiri & Delgutte, 2007; Chen, Rodriguez, Read, & Escabi, 2012). Along with the CF and CP, Bitds and BFitds were also spatially separable. Interestingly, the CDs were not spatially separable, indicating that both MSO and LSO inputs are affected by a similar range of “delay mechanisms,” regardless of how they are implemented.

Finally, the spatial segregation of ITD_{FS} properties was investigated in C1d to determine if there is a fine-grained representation embedded within this region of potent ITD responses. Unfortunately, the fractionation of this group was only 40 neurons, with few trough-type neurons. None of the ITD-sensitive parameters showed a spatial segregation when restricted to ITD_{FS} in this relatively small sample.

At the level of the IC, sensitivity to ITD_{FS} is entirely inherited from lower order auditory structures, as shown by comparing the response synchronies with the frequencies at each ear and the beat frequency using the binaural beat stimulus (Figure 11). In contrast, for ITD_{ENV} frequencies below a few hundred Hz, the synchrony to fluctuation at each ear could in theory account for the ITD sensitivity. However, the degree of synchrony shown to modulation frequencies in general is similar across IC neurons, monaural as well as binaural. Such sensitivity is expected from the first-spike latencies and slopes of phase-versus-modulation frequency plots, which both show temporal integration greater than that from lower centers, but not too great to resolve modulations up to several hundred Hz, as in other species (Joris, Schreiner, & Rees, 2004). In addition, the IC lacks the specialized mechanisms that exist at lower levels for extracting ITD information. Thus, although ITD_{ENV} could theoretically be extracted de novo in the IC (i.e., via non-MSO/LSO afferents or intrinsic connections), we think it more likely that sensitivity to ITD_{FS} and ITD_{ENV} are each inherited from lower level auditory nuclei.

A final issue is the sharpness of tuning to ITDs. By the level of the IC, the VS to beat frequencies is affected by both peripheral and central factors. The average VS in auditory nerve fibers to tone frequencies is about 0.70 to 0.80, corresponding to phase-locking that approximates the positive-going phases of tones (Rose, Brugge, Anderson, & Hind, 1967; Joris & Yin, 1992; Greenwood & Joris, 1996; Louage, van der Heijden, & Joris, 2004). In the cochlear nucleus there is a sharpening so that VS values >0.9 are seen (Joris, Carney, Smith, & Yin, 1994a; Joris, Smith, & Yin, 1994b). At the point of coincidence detection in the SOC, the cycle histograms to interaural phase are defined by the convolution between the two sides, and thus the VS is the product of that from each side (e.g., a VS of 0.9 to the stimulus frequency from both sides should produce a VS of 0.81 to the interaural phase at that frequency in an SOC neuron). Sharpening of ITD_{FS} processing between the IC and SOC has been described in the rabbit (Fitzpatrick, Kuwada, & Batra, 2002; Kuwada et al., 2006). The current results support similar sharpening in the gerbil. The VS in the gerbil's IC to beat frequencies was often very high, well above 0.9 in many cases. This high VS would not occur at the stage of coincidence detection of the SOC because of the multiplication from the two sides, as described above.

4.6 Implications for output pathways of the central nucleus

In Figure 1, a contrast was drawn between the pattern of connections in the mustached bat auditory pathway and the description in other species. The identification of relatively separate ITD-processing and non–ITD-processing areas in the gerbil IC gives rise to the two hypotheses shown in Figure 14. Either the projection from the central nucleus to the thalamic core has a single projection where the topography between the IC and thalamus is preserved (Figure 14a), which would be consistent with the single-pathway hypothesis of Figure 1A, or there is a reorganization according to the functional parcellation of ITD sensitivity (Figure 14b), which would be consistent with the data from the mustached bat, as in Figure 1B. A distinction between the mustached bat and other species, including the gerbil, is that the different functions vary according to frequency in the mustached bat, (e.g., frequency-modulated or constant frequency components of the biosonar signal; Figure 1b). In contrast, although ITD sensitivity and the pathways that support it dominate the low-

frequency realm, there are neurons with low CF where ITD sensitivity cannot be demonstrated, while sensitivity to ITD_{ENV} extends across the entire frequency range. Thus, functional relationships of areas and pathways in gerbils and most other species may be more difficult to dissociate from the underlying frequency organization than is the case in the mustached bat. Further studies will investigate these hypotheses, to shed light on the best representation of the pathways between the inferior colliculus and the auditory thalamus.

Acknowledgments

Funding information

National Institute on Deafness and Other Communication Disorders/National Institutes of Health, Grant/Award Numbers: R01 DC011347 and 5T32DC005360-12; National Institutes of Health, Grant/Award Numbers: NIH K01AG041211 and 1S10 ODOD010683-01; National Institute of Biomedical Imaging and Bioengineering/National Institutes of Health National Biomedical Technology Resource Center, Grant/Award Number: P41 EB015897

We thank Dr. G. Allan Johnson, Gary Cofer, and Yi Qi of the Duke Center for In Vivo Microscopy for their contributions to the gerbil MRI. We particularly thank Dr. Nell Cant at Duke University for her input and contributions to the development of this project, Dr. Julia Kimbell for her helpful instruction and comments on using the MIMICS software suite, and Dr. Shigeyuki Kuwada for his comments on an earlier version of the manuscript. We also thank two anonymous reviewers for their thoughtful comments.

References

Aitkin LM, Webster WR, Veale JL, Crosby DC. Inferior colliculus. I. Comparison of response properties of neurons in central, pericentral, and external nuclei of adult cat. Journal of Neurophysiology. 1975; 38:1196–1207. [PubMed: 1177012]

Badea A, Ali-Sharief AA, Johnson GA. Morphometric analysis of the C57BL/6J mouse brain. NeuroImage. 2007; 37:683–693. [PubMed: 17627846]

Badea A, Johnson GA, Williams RW. Genetic dissection of the mouse brain using high-field magnetic resonance microscopy. NeuroImage. 2009; 45:1067–1079. [PubMed: 19349225]

Batra R, Kuwada S, Stanford TR. Temporal coding of envelopes and their interaural delays in the inferior colliculus of the unanesthetized rabbit. Journal of Neurophysiology. 1989; 61:257–268. [PubMed: 2918354]

Batra R, Kuwada S, Stanford TR. High-frequency neurons in the inferior colliculus that are sensitive to interaural delays of amplitude-modulated tones: Evidence for dual binaural influences. Journal of Neurophysiology. 1993; 70:64–80. [PubMed: 8395589]

Batra R, Kuwada S, Fitzpatrick DC. Sensitivity to interaural temporal disparities of low- and high-frequency neurons in the superior olivary complex. II. Coincidence detection. Journal of Neurophysiology. 1997; 78:1237–1247. [PubMed: 9310415]

Bernstein LR. Auditory processing of interaural timing information: New insights. Journal of Neuroscience Research. 2001; 66:1035–1046. [PubMed: 11746435]

Blanks DA, Roberts JM, Buss E, Hall JW, Fitzpatrick DC. Neural and behavioral sensitivity to interaural time differences using amplitude modulated tones with mismatched carrier frequencies. Journal of the Association for Research in Otolaryngology. 2007; 8:393–408. [PubMed: 17657543]

Bruckner S, Rubsamen R. Binaural response characteristics in isofrequency sheets of the gerbil inferior colliculus. Hearing Research. 1995; 86:1–14. [PubMed: 8567406]

Cant NB. Patterns of convergence in the central nucleus of the inferior colliculus of the Mongolian gerbil: Organization of inputs from the superior olivary complex in the low frequency representation. Frontiers in Neural Circuits. 2013; 7:29. [PubMed: 23509001]

Cant NB, Benson CG. Parallel auditory pathways: Projection patterns of the different neuronal populations in the dorsal and ventral cochlear nuclei. Brain Research Bulletin. 2003; 60:457–474. [PubMed: 12787867]

Cant NB, Benson CG. An atlas of the inferior colliculus of the gerbil in three dimensions. Hearing Research. 2005; 206:12–27. [PubMed: 16080995]

Cant NB, Benson CG. Organization of the inferior colliculus of the gerbil (*Meriones unguiculatus*): Differences in distribution of projections from the cochlear nuclei and the superior olivary complex. The Journal of Comparative Neurology. 2006; 495:511–528. [PubMed: 16498677]

Cant NB, Benson CG. Organization of the inferior colliculus of the gerbil (*Meriones unguiculatus*): Projections from the cochlear nucleus. Neuroscience. 2008; 154:206–217. [PubMed: 18359572]

Chen C, Rodriguez FC, Read HL, Escabi MA. Spectro-temporal sound preferences of neighboring inferior colliculus neurons: Implications for local circuitry and processing. Frontiers in Neural Circuits. 2012; 6:62. [PubMed: 23060750]

Chernock ML, Larue DT, Winer JA. A periodic network of neurochemical modules in the inferior colliculus. Hearing Research. 2004; 188:12–20. [PubMed: 14759566]

Choy Buentello D, Bishop DC, Oliver DL. Differential distribution of GABA and glycine terminals in the inferior colliculus of rat and mouse. The Journal of Comparative Neurology. 2015; 523:2683–2697. [PubMed: 25976159]

Day ML, Koka K, Delgutte B. Neural encoding of sound source location in the presence of a concurrent, spatially separated source. Journal of Neurophysiology. 2012; 108:2612–2628. [PubMed: 22914651]

Dong, HW. The Allen reference atlas: A digital color brain atlas of the C57BL/6 male mouse. Hoboken, NJ: John Wiley & Sons; 2008.

Faye-Lund H, Osen KK. Anatomy of the inferior colliculus in rat. Anatomy and Embryology (Berlin). 1985; 171:1–20.

Felix RA 2nd, Magnusson AK, Berrebi AS. The superior paraolivary nucleus shapes temporal response properties of neurons in the inferior colliculus. Brain Structure and Function. 2015; 220:2639–2652. [PubMed: 24973970]

Fitzpatrick DC, Suga N, Olsen JF. Distribution of response types across entire hemispheres of the mustached bat's auditory cortex. The Journal of Comparative Neurology. 1998; 391:353–365. [PubMed: 9492205]

Fitzpatrick DC, Kuwada S, Batra R. Neural sensitivity to interaural time differences: Beyond the Jeffress model. The Journal of Neuroscience. 2000; 20:1605–1615. [PubMed: 10662850]

Fitzpatrick DC, Kuwada S, Batra R. Transformations in processing interaural time differences between the superior olivary complex and inferior colliculus: Beyond the Jeffress model. Hearing Research. 2002; 168:79–89. [PubMed: 12117511]

Fitzpatrick DC, Roberts JM, Kuwada S, Kim DO, Filipovic B. Processing temporal modulations in binaural and monaural auditory stimuli by neurons in the inferior colliculus and auditory cortex. Journal of the Association for Research in Otolaryngology. 2009; 10:579–593. [PubMed: 19506952]

Goldberg JM, Brown PB. Response of binaural neurons of dog superior olivary complex to dichotic tonal stimuli—Some physiological mechanisms of sound localization. Journal of Neurophysiology. 1969; 32:613–636. [PubMed: 5810617]

Greenwood DD, Joris PX. Mechanical and "temporal" filtering as codeterminants of the response by cat primary fibers to amplitude-modulated signals. The Journal of the Acoustical Society of America. 1996; 99:1029–1039. [PubMed: 8609286]

Grothe B, Pecka M, McAlpine D. Mechanisms of sound localization in mammals. Physiological Reviews. 2010; 90:983–1012. [PubMed: 20664077]

Hancock KE, Delgutte B. A physiologically based model of interaural time difference discrimination. The Journal of Neuroscience. 2004; 24:7110–7117. [PubMed: 15306644]

Hutson, KA. The ipsilateral auditory pathway: A psychobiological perspective. In: Christman, S., editor. Cerebral asymmetries in sensory and perceptual processing. New York: Elsevier; 1997. p. 383-468.Advances in Psychology

Irvine, DRF. Physiology of the auditory brainstem. In: Popper, AN., Fay, RR., editors. The mammalian auditory pathway: Neurophysiology. New York: Springer; 1992. p. 153-231.

Johnson GA, Cofer GP, Fubara B, Gewalt SL, Hedlund LW, Maronpot RR. Magnetic resonance histology for morphologic phenotyping. Journal of Magnetic Resonance Imaging. 2002a; 16:423–429. [PubMed: 12353257]

Johnson GA, Cofer GP, Gewalt SL, Hedlund LW. Morphologic phenotyping with MR microscopy: The visible mouse. Radiology. 2002b; 222:789–793. [PubMed: 11867802]

Johnson GA, Badea A, Brandenburg J, Cofer G, Fubara B, Liu S, Nissanov J. Waxholm space: An image-based reference for coordinating mouse brain research. NeuroImage. 2010; 53:365–372. [PubMed: 20600960]

Joris PX, Yin TC. Responses to amplitude-modulated tones in the auditory nerve of the cat. The Journal of the Acoustical Society of America. 1992; 91:215–232. [PubMed: 1737873]

Joris PX, Carney LH, Smith PH, Yin TC. Enhancement of neural synchronization in the anteroventral cochlear nucleus. I. Responses to tones at the characteristic frequency. Journal of Neurophysiology. 1994a; 71:1022–1036. [PubMed: 8201399]

Joris PX, Smith PH, Yin TC. Enhancement of neural synchronization in the anteroventral cochlear nucleus. II. Responses in the tuning curve tail. Journal of Neurophysiology. 1994b; 71:1037–1051. [PubMed: 8201400]

Joris PX, Schreiner CE, Rees A. Neural processing of amplitude-modulated sounds. Physiological Reviews. 2004; 84:541–577. [PubMed: 15044682]

Kaas JH, Hackett TA. Subdivisions of auditory cortex and processing streams in primates. Proceedings of the National Academy of Sciences of the United States of America. 2000; 97:11793–11799. [PubMed: 11050211]

Kelly JB, Glenn SL, Beaver CJ. Sound frequency and binaural response properties of single neurons in rat inferior colliculus. Hearing Research. 1991; 56:273–280. [PubMed: 1769920]

Kiang NY, Moxon EC. Tails of tuning curves of auditory-nerve fibers. The Journal of the Acoustical Society of America. 1974; 55:620–630. [PubMed: 4819862]

Konishi M. Coding of auditory space. Annual Review of Neuroscience. 2003; 26:31–55.

Kuwada S, Yin TC, Wickesberg RE. Response of cat inferior colliculus neurons to binaural beat stimuli: Possible mechanisms for sound localization. Science. 1979; 206:586–588. [PubMed: 493964]

Kuwada S, Stanford TR, Batra R. Interaural phase-sensitive units in the inferior colliculus of the unanesthetized rabbit: Effects of changing frequency. Journal of Neurophysiology. 1987; 57:1338–1360. [PubMed: 3585471]

Kuwada S, Fitzpatrick DC, Batra R, Ostapoff EM. Sensitivity to interaural time differences in the dorsal nucleus of the lateral lemniscus of the unanesthetized rabbit: Comparison with other structures. Journal of Neurophysiology. 2006; 95:1309–1322. [PubMed: 16338997]

Loftus WC, Bishop DC, Saint Marie RL, Oliver DL. Organization of binaural excitatory and inhibitory inputs to the inferior colliculus from the superior olive. The Journal of Comparative Neurology. 2004; 472:330–344. [PubMed: 15065128]

Loftus WC, Malmierca MS, Bishop DC, Oliver DL. The cytoarchitecture of the inferior colliculus revisited: A common organization of the lateral cortex in rat and cat. Neuroscience. 2008; 154:196–205. [PubMed: 18313229]

Loftus WC, Bishop DC, Oliver DL. Differential patterns of inputs create functional zones in central nucleus of inferior colliculus. The Journal of Neuroscience. 2010; 30:13396–13408. [PubMed: 20926666]

Lomber SG, Malhotra S. Double dissociation of ‘what’ and ‘where’ processing in auditory cortex. Nature Neuroscience. 2008; 11:609–616. [PubMed: 18408717]

Louage DH, van der Heijden M, Joris PX. Temporal properties of responses to broadband noise in the auditory nerve. Journal of Neurophysiology. 2004; 91:2051–2065. [PubMed: 15069097]

Malhotra S, Hall AJ, Lomber SG. Cortical control of sound localization in the cat: Unilateral cooling deactivation of 19 cerebral areas. Journal of Neurophysiology. 2004; 92:1625–1643. [PubMed: 15331649]

Malmierca MS, Saint Marie RL, Merchan MA, Oliver DL. Laminar inputs from dorsal cochlear nucleus and ventral cochlear nucleus to the central nucleus of the inferior colliculus: Two patterns of convergence. Neuroscience. 2005; 136:883–894. [PubMed: 16344158]

Malmierca MS, Izquierdo MA, Cristaudo S, Hernandez O, Perez-Gonzalez D, Covey E, Oliver DL. A discontinuous tono-topic organization in the inferior colliculus of the rat. The Journal of Neuroscience. 2008; 28:4767–4776. [PubMed: 18448653]

Malmierca MS, Hernandez O, Antunes FM, Rees A. Divergent and point-to-point connections in the commissural pathway between the inferior colliculi. The Journal of Comparative Neurology. 2009; 514:226–239. [PubMed: 19296464]

Mardia, KV., Jupp, PE. Directional statistics. Hoboken, NJ: John Wiley & Sons; 2000.

Marshall AF, Pearson JM, Falk SE, Skaggs JD, Crocker WD, Saldana E, Fitzpatrick DC. Auditory response properties of neurons in the tectal longitudinal column of the rat. Hearing Research. 2008; 244:35–44. [PubMed: 18662764]

McAlpine D, Jiang D, Palmer AR. Interaural delay sensitivity and the classification of low best-frequency binaural responses in the inferior colliculus of the guinea pig. Hearing Research. 1996; 97:136–152. [PubMed: 8844194]

Meijering, EHW. TransformJ. Lausanne, Switzerland: Biomedical Imaging Group, Swiss Federal Institute of Technology; 2000–2002.

Moore DR, Kitzes LM. Projections from the cochlear nucleus to the inferior colliculus in normal and neonatally cochlea-ablated gerbils. The Journal of Comparative Neurology. 1985; 240:180–195. [PubMed: 4056109]

Oliver DL, Morest DK. The central nucleus of the inferior colliculus in the cat. The Journal of Comparative Neurology. 1984; 222:237–264. [PubMed: 6699209]

Oliver, DL., Huerta, MF. Inferior and superior colliculi. In: Webster, DB.Popper, AN., Fay, RR., editors. The mammalian auditory pathway: Neuroanatomy. New York: Springer; 1992. p. 168-221.

Oliver DL, Kuwada S, Yin TC, Haberly LB, Henkel CK. Dendritic and axonal morphology of HRP-injected neurons in the inferior colliculus of the cat. The Journal of Comparative Neurology. 1991; 303:75–100. [PubMed: 2005240]

Olsen JF, Suga N. Combination-sensitive neurons in the medial geniculate body of the mustached bat: Encoding of relative velocity information. Journal of Neurophysiology. 1991a; 65:1254–1274. [PubMed: 1875241]

Olsen JF, Suga N. Combination-sensitive neurons in the medial geniculate body of the mustached bat: Encoding of target range information. Journal of Neurophysiology. 1991b; 65:1275–1296. [PubMed: 1651998]

O'Neill WE, Suga N. Target range-sensitive neurons in the auditory cortex of the mustache bat. Science. 1979; 203:69–73. [PubMed: 758681]

Palmer, AR., Kuwada, S. Binaural and spatial coding in the inferior colliculus. In: Winer, JA., Schreiner, CE., editors. The inferior colliculus. New York: Springer; 2005. p. 377-410.

Pearson JM, Crocker WD, Fitzpatrick DC. Connections of functional areas in the mustached bat's auditory cortex with the auditory thalamus. The Journal of Comparative Neurology. 2007; 500:401–418. [PubMed: 17111381]

Plauska A, Borst JG, van der Heijden M. Predicting binaural responses from monaural responses in the gerbil medial superior olive. Journal of Neurophysiology. 2016; 115:2950–2963. [PubMed: 27009164]

Popelar J, Syka J. Response properties of neurons in the inferior colliculus of the guinea-pig. Acta Neurobiologiae Experimentalis. 1982; 42:299–310. [PubMed: 7184324]

Portfors CV, Wenstrup JJ. Topographical distribution of delay-tuned responses in the mustached bat inferior colliculus. Hearing Research. 2001; 151:95–105. [PubMed: 11124455]

Rasband, WS. ImageJ. Bethesda, MD: US National Institutes of Health; 1997–2014.

Rauschecker JP. Auditory and visual cortex of primates: A comparison of two sensory systems. European Journal of Neuroscience. 2015; 41:579–585. [PubMed: 25728177]

Recanzone GH, Cohen YE. Serial and parallel processing in the primate auditory cortex revisited. Behavioural Brain Research. 2010; 206:1–7. [PubMed: 19686779]

Rose JE, Brugge JF, Anderson DJ, Hind JE. Phase-locked response to low-frequency tones in single auditory nerve fibers of the squirrel monkey. Journal of Neurophysiology. 1967; 30:769–793. [PubMed: 4962851]

Roth GL, Aitkin LM, Andersen RA, Merzenich MM. Some features of the spatial organization of the central nucleus of the inferior colliculus of the cat. The Journal of Comparative Neurology. 1978; 182:661–680. [PubMed: 721973]

Saldaña E, Merchán MA. Intrinsic and commissural connections of the rat inferior colliculus. The Journal of Comparative Neurology. 1992; 319:417–437. [PubMed: 1376335]

Schreiner CE, Langner G. Periodicity coding in the inferior colliculus of the cat. II. Topographical organization. Journal of Neurophysiology. 1988; 60:1823–1840. [PubMed: 3236053]

Semple MN, Aitkin LM. Representation of sound frequency and laterality by units in central nucleus of cat inferior colliculus. Journal of Neurophysiology. 1979; 42:1626–1639. [PubMed: 501392]

Semple MN, Kitzes LM. Single-unit responses in the inferior colliculus: Cifferent consequences of contralateral and ipsilateral auditory stimulation. Journal of Neurophysiology. 1985; 53:1467–1482. [PubMed: 4009228]

Seshagiri CV, Delgutte B. Response properties of neighboring neurons in the auditory midbrain for pure-tone stimulation: A tetrode study. Journal of Neurophysiology. 2007; 98:2058–2073. [PubMed: 17671101]

Shackleton TM, McAlpine D, Palmer AR. Modelling convergent input onto interaural-delay-sensitive inferior colliculus neurones. Hearing Research. 2000; 149:199–215. [PubMed: 11033259]

Spitzer MW, Semple MN. Responses of inferior colliculus neurons to time-varying interaural phase disparity: Effects of shifting the locus of virtual motion. Journal of Neurophysiology. 1993; 69:1245–1263. [PubMed: 8492161]

Spitzer MW, Semple MN. Neurons sensitive to interaural phase disparity in gerbil superior olive: Diverse monaural and temporal response properties. Journal of Neurophysiology. 1995; 73:1668–1690. [PubMed: 7643174]

Spitzer MW, Semple MN. Transformation of binaural response properties in the ascending auditory pathway: Influence of time-varying interaural phase disparity. Journal of Neurophysiology. 1998; 80:3062–3076. [PubMed: 9862906]

Suga N, O'Neill WE, Kujirai K, Manabe T. Specificity of combination-sensitive neurons for processing of complex biosonar signals in auditory cortex of the mustached bat. Journal of Neurophysiology. 1983; 49:1573–1626. [PubMed: 6875639]

van der Heijden M, Lorteije JA, Plauska A, Roberts MT, Golding NL, Borst JG. Directional hearing by linear summation of binaural inputs at the medial superior olive. Neuron. 2013; 78:936–948. [PubMed: 23764292]

Vonderschen K, Wagner H. Detecting interaural time differences and remodeling their representation. Trends in Neuroscience. 2014; 37:289–300.

Wallace MN, Shackleton TM, Palmer AR. Morphological and physiological characteristics of laminar cells in the central nucleus of the inferior colliculus. Frontiers in Neural Circuits. 2012; 6:55. [PubMed: 22933991]

Wenstrup JJ. Frequency organization and responses to complex sounds in the medial geniculate body of the mustached bat. Journal of Neurophysiology. 1999; 82:2528–2544. [PubMed: 10561424]

Wenstrup JJ, Grose CD. Inputs to combination-sensitive neurons in the medial geniculate body of the mustached bat: The missing fundamental. The Journal of Neuroscience. 1995; 15:4693–4711. [PubMed: 7540682]

Wenstrup JJ, Ross LS, Pollak GD. Binaural response organization within a frequency-band representation of the inferior colliculus: Implications for sound localization. The Journal of Neuroscience. 1986; 6:962–973. [PubMed: 3701417]

Wenstrup JJ, Larue DT, Winer JA. Projections of physiologically defined subdivisions of the inferior colliculus in the mustached bat: Targets in the medial geniculate body and extrathalamic nuclei. The Journal of Comparative Neurology. 1994; 346:207–236. [PubMed: 7962717]

Wenstrup JJ, Mittmann DH, Grose CD. Inputs to combination-sensitive neurons of the inferior colliculus. The Journal of Comparative Neurology. 1999; 409:509–528. [PubMed: 10376737]

Willard FH, Martin GF. The auditory brainstem nuclei and some of their projections to the inferior colliculus in the North American opossum. Neuroscience. 1983; 10:1203–1232. [PubMed: 6664491]

Winer, JA., Schreiner, CE., editors. The inferior colliculus. New York: Springer-Verlag; 2005.

Wong-Riley MTT. Endogenous peroxidatic activity in brain stem neurons as demonstrated by their staining with diaminobenzidine in normal squirrel monkeys. Brain Research. 1976; 108:257–277. [PubMed: 819097]

Yin TC, Chan JC. Interaural time sensitivity in medial superior olive of cat. Journal of Neurophysiology. 1990; 64:465–488. [PubMed: 2213127]

Yin TC, Kuwada S. Binaural interaction in low-frequency neurons in inferior colliculus of the cat. II. Effects of changing rate and direction of interaural phase. Journal of Neurophysiology. 1983a; 50:1000–1019. [PubMed: 6631458]

Yin TC, Kuwada S. Binaural interaction in low-frequency neurons in inferior colliculus of the cat. III. Effects of changing frequency. Journal of Neurophysiology. 1983b; 50:1020–1042. [PubMed: 6631459]

Yin, TC., Chan, JC., Kuwada, S. Characteristic delays and their topographical distribution in the inferior colliculus of the cat. In: Webster, WR., Aitkin, LM., editors. Mechanisms of hearing. Clayton, Australia: Monash University Press; 1983. p. 94-99.

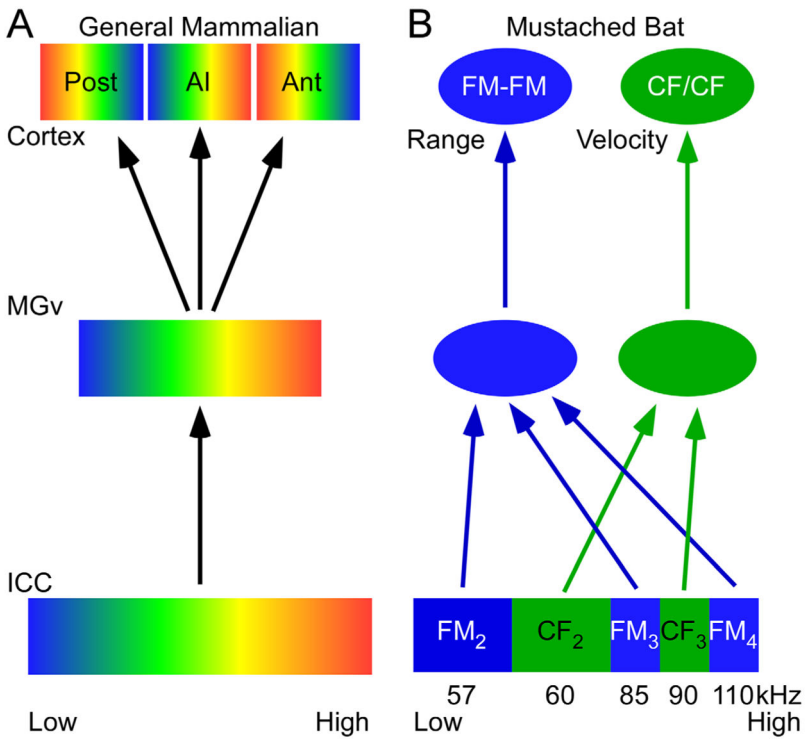

FIGURE 1.

Schematics of pathways between the central nucleus of the IC and the core areas of the auditory cortex. (a) General mammalian pattern. The pathway from the central nucleus is usually depicted as a single output to the ventral division of the medial geniculate body (MGv) and from there to multiple tonotopic areas of the auditory core, including the primary auditory cortex (AI) and, for example, regions anterior (Ant) and posterior (Post) to AI. (b) The mustached bat. As in other species, the central nucleus of the IC has a single tonotopic representation. Because of the specializations for biosonar, different frequencies serve different functions according to their role in the analysis of the emitted signal and its echoes. Regions sensitive to frequency-modulated components of different harmonics (FM_2, FM_3, and FM_4) of the biosonar signal process target range. Neurons sensitive to constant frequency components (CF_2 and CF_3) process target velocity, among other features. The outputs of the IC reorganize these features so that, in the MGv and cortex, the properties that were distributed according to frequency in the central nucleus become organized into “functional areas” at the thalamic and cortical levels

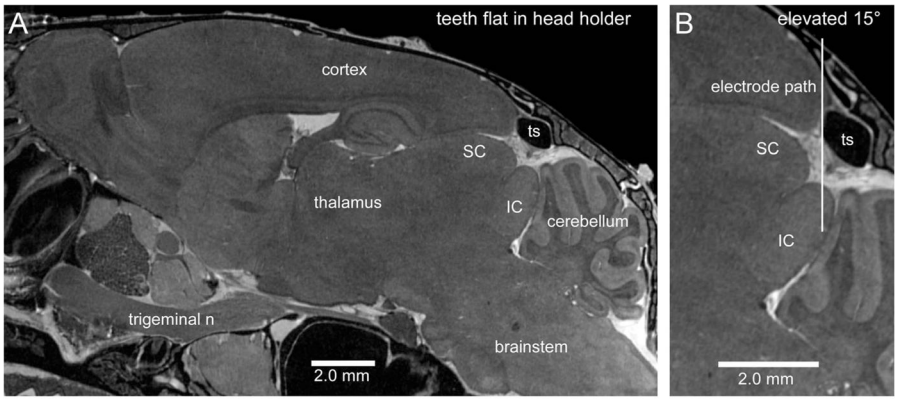

FIGURE 2.

Orientation of the brain for physiology experiments. (a) Parasagittal MRI section showing the approximate orientation of the gerbil brain in the stereotactic head holder. (b) To avoid puncture of the transverse sinus (ts), we elevate the head holder 15 degrees. IC, inferior colliculus; SC, superior colliculus. Scale bar =2 mm in A,B.

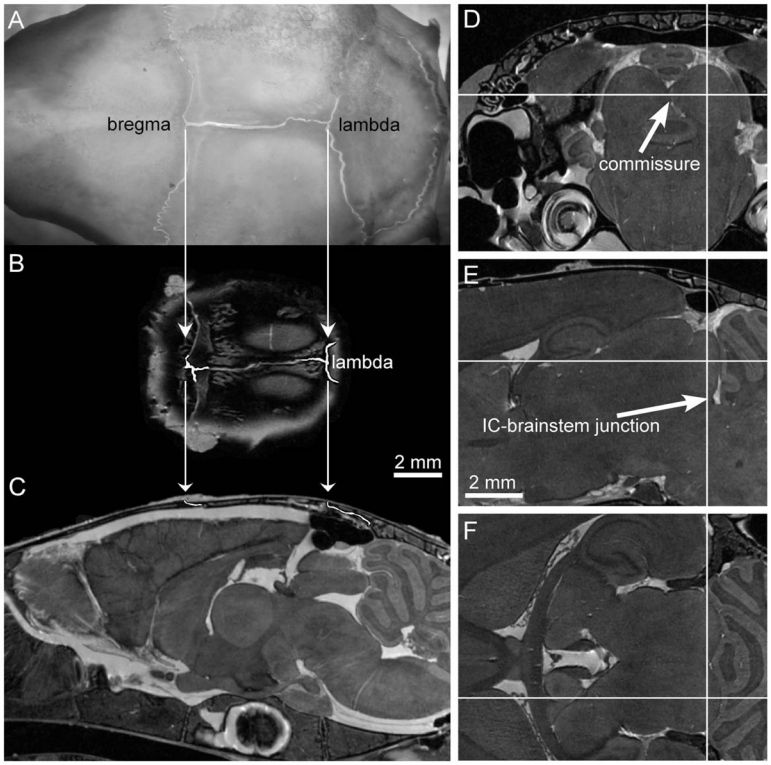

FIGURE 3.

Establishing coordinate points for zero in MRI space (a–c) and registration points for section alignment (d–f). The left panels show a photograph of a gerbil skull (a) in reference to an MRI series that has been rotated such that lambda and bregma lie in the same horizontal plane (b,c). Lambda was chosen as the zero point for the locations of physiological recording sites as it can be seen on the dorsal surface of the skull and can be readily identiifed in MR images in horizontal (b) and sagittal (c) planes. Arrows point to lambda in both. Lambda and bregma have been digitally enhanced in the MRI panels for clarity. The right panels are images from our standard MRI orientation, showing a region containing the IC in three cardinal planes (d, coronal; e, sagittal; f, horizontal) and the internal structures used to align histological sections to the MRI (arrows in d and e). Using ImageJ's orthogonal views function, cross-hairs can be placed at any location (e.g., the IC in f) and automatically render the other two planes of section at the intersecting coordinates. Scale bar =2 mm in B (applies to a–c) and e (applies to d–f).

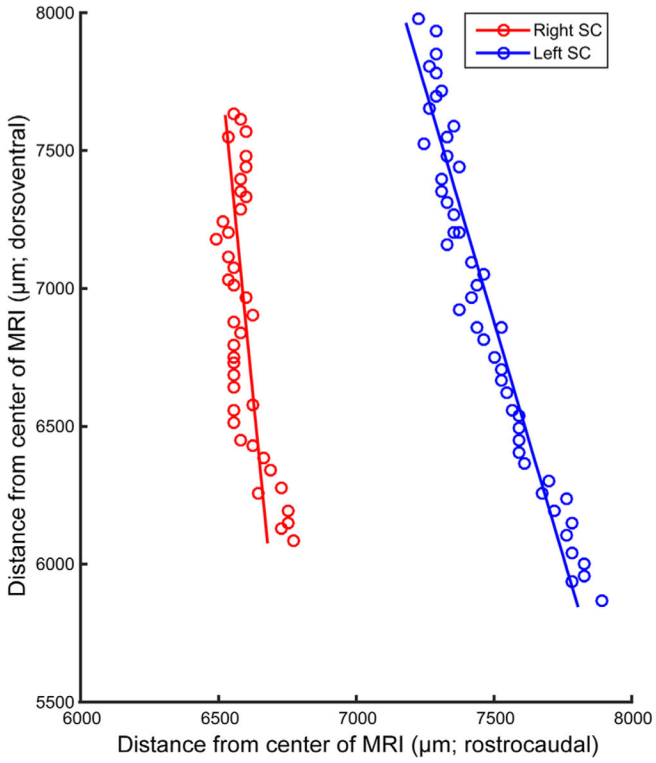

FIGURE 4.

Accuracy of tissue alignment into MRI space. Two 29-gauge tubes stereotactically lowered into a gerbil brain at different locations and different penetration angles to produce fiduciary points that could be recovered in tissue sectioned in the horizontal plane. The scatter plots show sagittal reconstructions of the trajectories of each penetration. The ordinate shows the location along the dorsoventral axis of the superior colliculus (SC); the abscissa represents the caudorostral location within the MRI framework. Red circles indicate holes made in the right hemisphere, blue circles in the left hemisphere. The solid lines are bestfit lines derived using Deming (orthogonal) regression. The difference between the angles was 10.76°, versus the actual stereotactically adjusted 10°

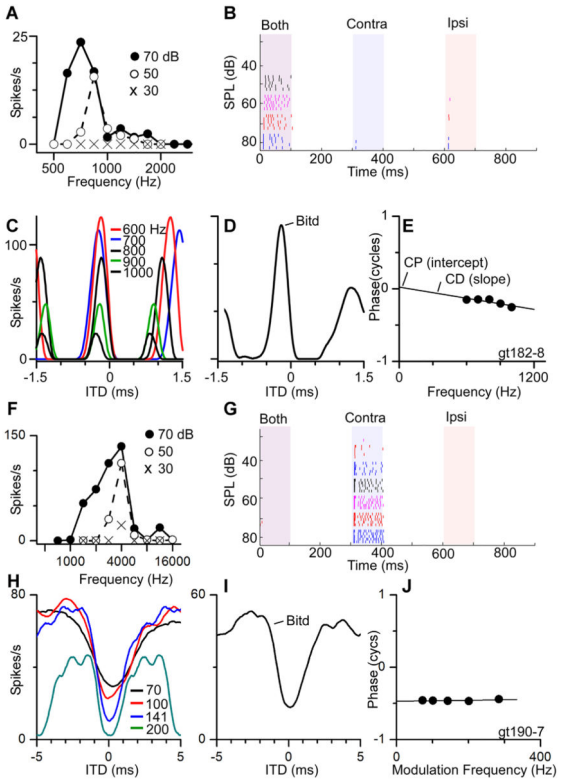

FIGURE 5.

Examples of interaural time difference (ITD)-sensitive responses. (a–e) A low-frequency neuron with tuning to fine structure ITDs. (a) Frequency tuning. The characteristic frequency (CF), or frequency of maximum response at the lowest intensity with a response, was 841 Hz. The BF70, or frequency with the maximal response at 70 dB SPL, was 700 Hz. (b) Level series at CF, showing responses to binaural and monaural stimulation. This response pattern is EE/F. (c) Delay curves to a 1-Hz binaural beat, showing a strong "peaker" type of ITD sensitivity. (d) Composite ITD curve showing the average Bitd (−190 μs) for this unit. (e) Composite phase-frequency plot derived from the phase curve in C; this unit had a characteristic phase (CP) near zero and a characteristic delay (CD) of −240 μs (see text for details). (f–j) A high-frequency CF neuron (4,000 Hz) driven primarily by the contralateral ear that showed strong inhibition upon binaural stimulation, characterized as an EO/I type neuron (f,g). Sine amplitude modulated (SAM) tones demonstrate sensitivity to ITD envelope, and a "trougher" type response (h,i), with a Bitd of −2,600 μs, consistent with a CD near 77 μs and CP of −0.47 cycles (j)

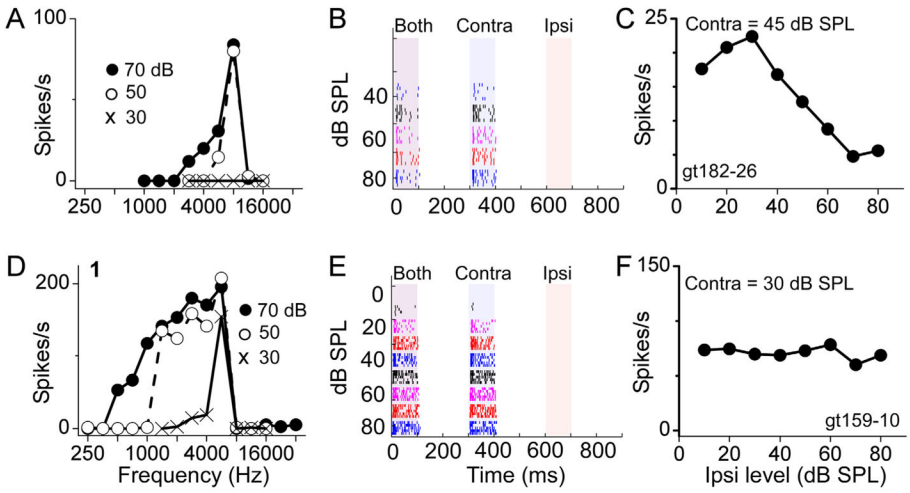

FIGURE 6.

Non-ITD sensitive units. (a–c) Unit with a CF of 8,000 Hz (a), which was excited by contralateral stimulation, no response to the ipsilateral stimulation, yet slightly inhibited by binaural stimuli (b). This was an EO/I type response, confirmed by holding the contralateral stimulus at constant amplitude and varying the level at the ipsilateral ear (c). This neuron showed no ITD sensitivity to tone, noise, or SAM beats. (d–f) This neuron (CF of 5,700 Hz; d) behaved similar to the unit in a, being strongly excited by contralateral stimulation, but no response or change in the response to ipsilateral stimulation (e,f). This neuron also showed no ITD sensitivity and was typed as EO/O, or a monaural unit

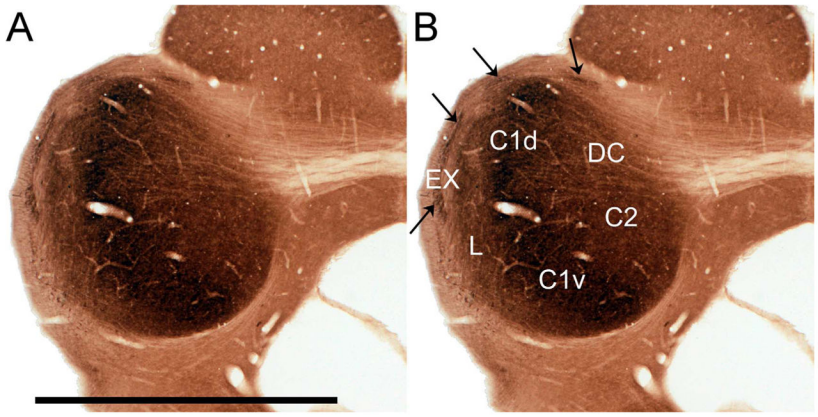

FIGURE 7.

Levels of cytochrome oxidase activity in the IC can be used to subdivide the IC into its constituent subregions.

Photomicrograph of a representative IC section without (a) and with (b) subdivision labels. In the present study, we report observations from six regions. The central region of densest CO represents zone 1 (c1) of the central nucleus, and is further subdivided into dorsal (c1d) and ventral (c1v) parts. Less dense CO activity medial to C1 is zone 2 of the central nucleus (c2), and the dorsal cortex (DC). The lateral nucleus (L) and the external cortex (EX) are the lateralmost subdivisions of the IC. Arrows indicate examples of “islands” of high CO activity within the fibrous structure of EX. Medial is right, and dorsal is up. Scale bar =2 mm in a (applies to a,b)

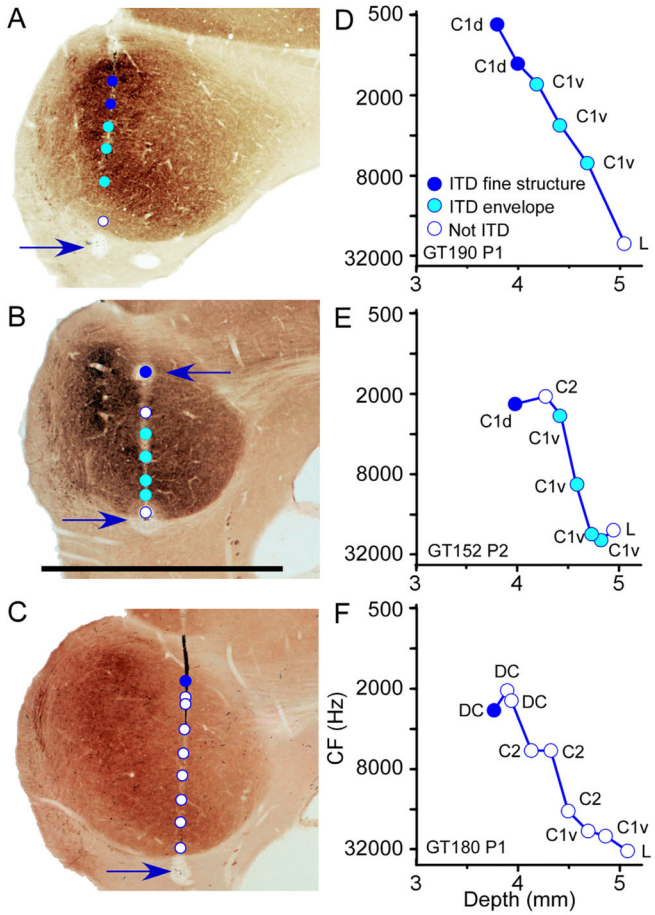

FIGURE 8.

Recovery of recording sites in physiology experiments. (a–c) CO-stained sections through the IC from three animals showing the electrode penetration in each case overlaid with the location of recording sites of individual units, obtained relative to the location of electrolytic lesions made at the end of the penetration (arrows). Blue and cyan circles indicate the type of ITD-sensitive units (ITD_{FS} vs. ITD_{ENV}), and white circles represent units that did not respond to our battery of ITD tests. (d–f) The location of each recording site (abscissa) is plotted against its central frequency (ordinate). Recording sites are colored as on the left, and labeled with their locations in the histology, with d corresponding to a and so on. Medial is to the right, and dorsal is at the top in each of the histology photomicrographs. Scale bar =2 mm in b (applies to a–c)

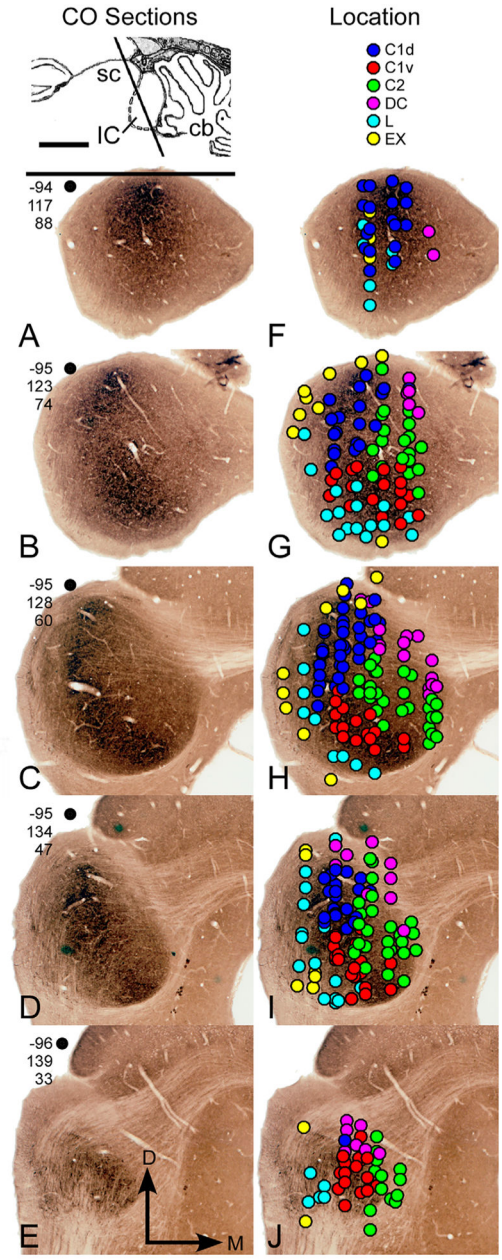

FIGURE 9.

Recording site locations and physiological data from individual cases (e.g., Fig. 7) pooled across all animals. Inset at upper left shows the approximate plane of section through the IC using an illustration derived from a sagittal image of the MRI stack (cb, cerebellum). (a–**e)** Five coronal sections from a separate atlas brain, spaced 320 μm apart, arranged caudal (a) to rostral (e). (f–j) The same sections, overlaid with recording sites from physiological experiments. Each site is color coded with their locations in their original histology (legend). Blue, C1d; red, C1v; green, C2; magenta, DC; cyan, L; yellow, EX. a–e are labeled with a black dot and the three axial coordinate numbers that define that dot in MRI space, with the origin at the lambda point, and positive coordinates being to the right, ventral, and rostral.

Aligning the dots would orient the images within the MRI space at the estimated angle of section. Scale bar =2 mm in a (applies to a–j)

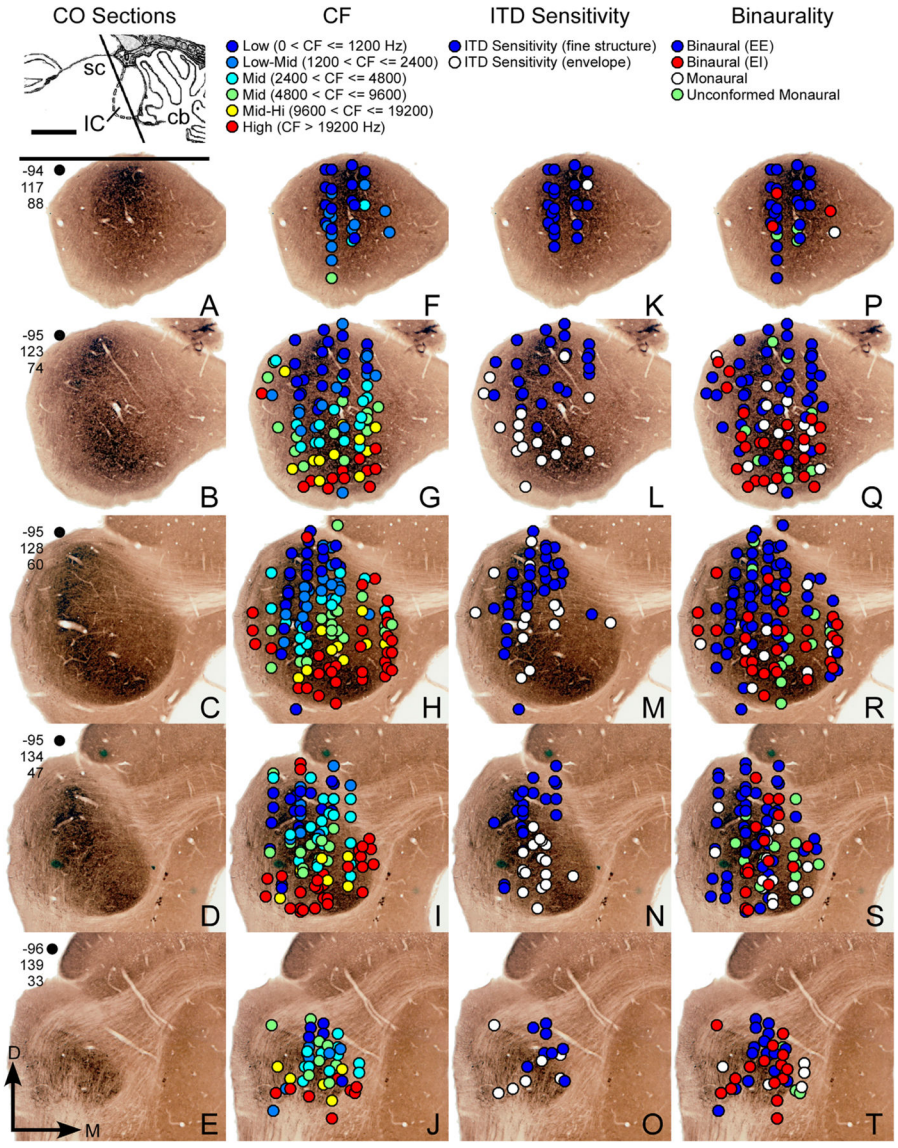

FIGURE 10.

(a–t) Physiological response properties (characteristic frequency [CF], ITD sensitivity, and binaurality) from the recording sites shown in Figure 8. As in Figure 8, the left column (a–e) is an orientation series of CO-stained IC sections. Above each column is a color-coded legend to identify the type of response property illustrated in that column. Note: for some response properties, e.g., ITD, not all units had an ITD response and are therefore not represented. Scale bar =2 mm in a (applies to a–t)

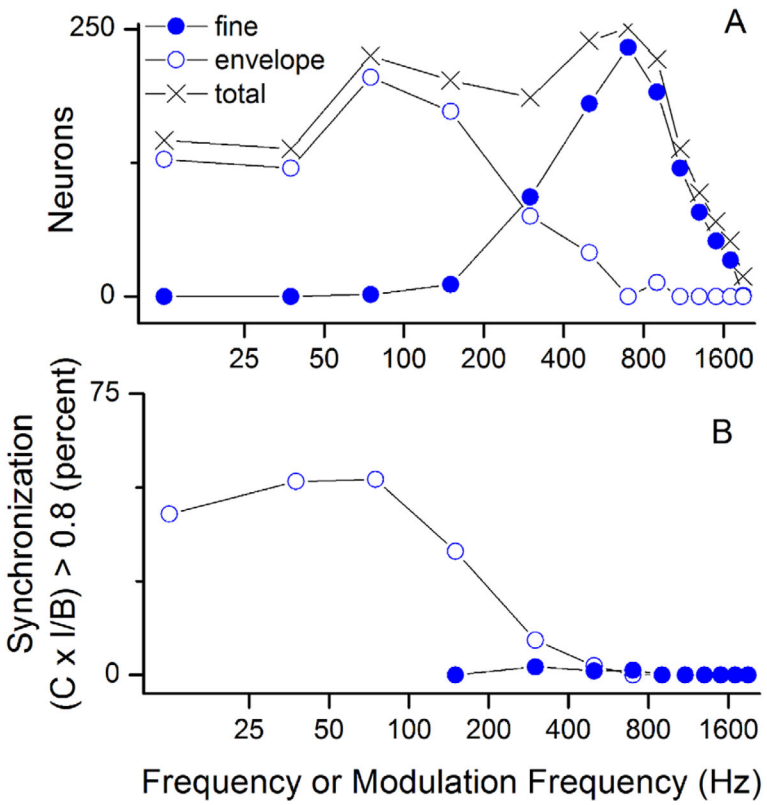

FIGURE 11.

Frequency representation and synchronization rates in ITD processing. (a) Number of neurons at each frequency that respond to ITD fine structure or envelope. Note that fine structure ends at approximately 1,600 Hz (highest level of phase locking), but ITD to envelopes continues into very low modulation frequencies. (b) Synchronization rate relationships comparing fine and envelope ITD sensitivity, suggesting that primary binaural interactions may still be possible at the level of IC for envelope sensitivity but not for fine structure

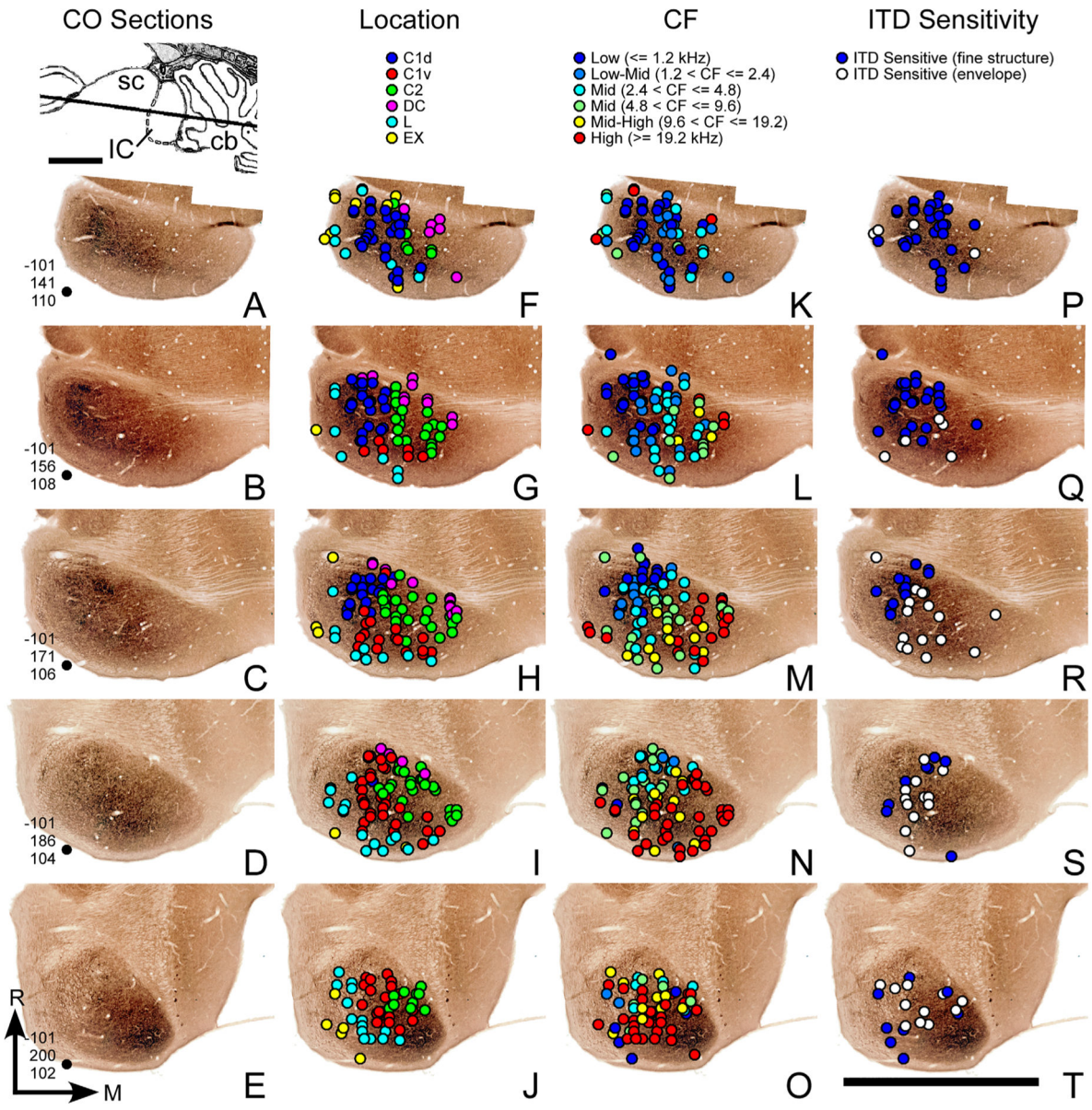

FIGURE 12.

(a–t) Data from Figures 9 and 10 replotted in a horizontal orientation (upper left inset is derived from a sagittal image in the MRI stack showing the plane of section relative to the IC). As in Figures 9 and 10, coordinates of the black dot are relative to lambda; aligning the black dot would arrange the images in their estimated plane of section. See legends to Figures 9 and 10. Scale bar =2 mm in t (applies to a–t)

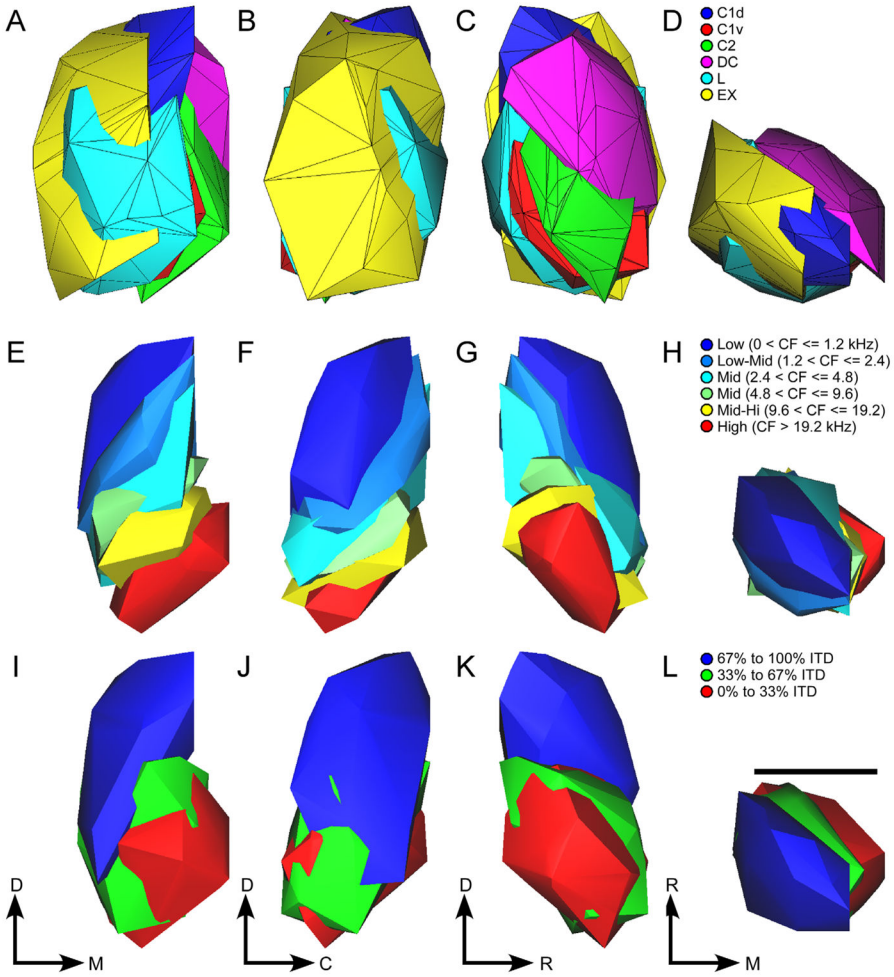

FIGURE 13.

Three-dimensional renderings of results. (a–d) Surface depictions of the areas of the gerbil's IC. Triangulated from the location data of recording sites (see Fig. 8f–j). (e–h) Surface depictions of frequency laminae in the central nucleus (C1d, C1, and C2). Derived from the CFs of physiological recording sites (see Fig. 10f–j). (i–l) Surface depiction of the degree of ITD sensitivity in the central nucleus, derived by dividing the central nucleus into cubes with 320-μm sides and calculating the percentage of cells in each cube that were ITD sensitive. a, e, and i are coronal orientations; b, f, and j, and c, g, and k are both sagittal orientations, with one rotated 180° from the other (see orientation arrows at the bottom); d, h, and l are horizontal orientations. Scale bar =1 mm in l (applies to a–l)

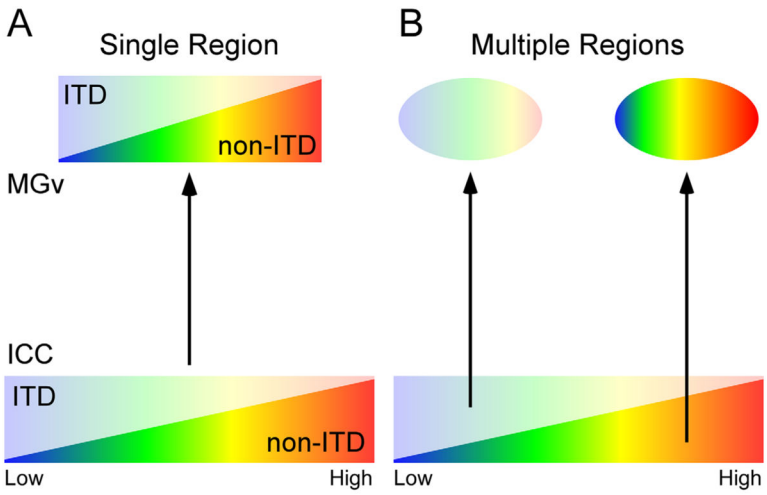

FIGURE 14.

Schematics of possible pathways between the central nucleus of the IC and the core areas of the auditory cortex. Both start from an IC where the ITD-sensitive regions are localized to separate parts of the frequency lamina, although not strictly orthogonal, i.e., more low CF neurons are ITD-sensitive than high CF neurons. (a) The pathway according to the general mammalian plan shown in Figure 1a. (b) The pathway according to the pattern in mustached bat, where there is a transformation from an organization according to frequency to one according to function

TABLE 1

Percentages of neurons in each division of the inferior colliculus with particular response properties

	Count	Bin (%)	Mon (%)	ITD (%)	Not ITD (%)	FS (%)	ENV (%)
C1d	94	89.4	3.2	81.9	7.4	68.1	13.8
C1v	68	64.7	19.1	45.6	19.1	10.3	35.3
C2	89	62.9	20.2	16.9	46.1	11.2	5.6
L	51	76.5	11.8	27.5	49.0	11.8	15.7
DC	39	82.1	10.3	33.3	48.7	30.8	2.6
EX	31	90.3	6.5	58.1	32.3	45.2	12.9
Totals	372[a]	76.1[b]	12.4[b]	45.2[c]	30.9[c]	30.4[d]	14.8[d]

DC =dorsal cortex; EX =external nucleus; ITD =interaural time difference; L =lateral nucleus.

[a]Of the 386 units studied, 372 received sufficient testing for the analyses presented in the table.

[b]11.5% of neurons were not sufficiently tested to rule out binaurality.

[c]23.9% of neurons were not sufficiently tested to rule out ITD sensitivity.

[d]These total 45.2%, or the proportion of ITD-sensitive neurons.

TABLE 2

Fine structure ITD properties divided by type

		ITD properties (mean (SD))					
ITD type	**No.**	**Bitd (μs)**	**CD (μs)**	**CP (cyc)**	**BFitd (Hz)**	**Max sync**	**Mean sync**
Peak	31	110 (80)	81 (80)	0.06 (0.03)	730.22 (254.31)	0.77 (0.18)	0.56 (0.18)
Intermediate	15	220 (80)	69 (80)	0.22 (0.09)	792.37 (158.85)	0.85 (0.13)	0.70 (0.18)
Trough	9	310 (120)	30 (250)	0.40 (0.18)	767.32 (180.81)	0.64 (0.25)	0.44 (0.17)
ANOVAs	F	22.53	1.12	57.7	0.41	3.5	6.5
df 2, 51	*P*	<0.001	0.36	<0.001	0.66	0.039	0.003

BFitd =best frequency for ITD sensitivity; Bitd =best ITD; CD =characteristic delay; CP =characteristic phase; ITD =interaural time difference.

TABLE 3

Envelope ITD properties divided by type

		ITD properties (mean (SD))					
ITD type	**No.**	**Bitd (μs)**	**CD (μs)**	**CP (cyc)**	**BFitd (Hz)**	**Max sync**	**Mean sync**
Peak	8	1160 (800)	390 (230)	0.07 (0.04)	152.04 (152.04)	0.36 (0.11)	0.27 (0.10)
Intermediate	6	4060 (1890)	220 (300)	0.31 (0.04)	71.32 (23.65)	0.34 (0.15)	0.29 (0.15)
Trough	30	8900 (9630)	910 (2050)	0.41 (0.11)	89.61 (74.62)	0.57 (0.20)	0.45 (0.20)
ANOVAs	F	3.26	0.59	40.6	1.86	6.8	4.3
df 2, 41	p	0.048	0.56	<0.001	0.168	0.003	0.002

BFitd =best frequency for ITD sensitivity; Bitd =best ITD; CD =characteristic delay; CP =characteristic phase; ITD =interaural time difference.

TABLE 4

ANOVA for first spike latency across inferior colliculus subregions

Group	No.	FS latency (ms) (mean (SD))
C1d	98	12.1 (7.54)
C1v	74	9.8 (5.74)
C2	90	11.0 (5.59)
DC	41	13.7 (7.30)
L	52	14.3 (8.19)
EX	31	19.1 (11.1)
ANOVAs	F	8.81
df 5, 380	*P*	<0.001

DC =dorsal cortex; EX =external nucleus; L =lateral nucleus.